AGU PUBLICATIONS

JGR

Journal of Geophysical Research: Oceans

RESEARCH ARTICLE

10.1002/2016JC012306

Key Points:
- We measured gross and net productivity using a combination of in situ gas tracer, incubation, and sediment trap methods in Monterey Bay
- Net community production estimates from oxygen/argon ratios and nitrate incubations agreed very well when the system was at steady state
- Following the arrival of recently upwelled water to the study area, incubation-based carbon and nitrogen uptake increased

Supporting Information:
- Supporting Information S1
- Data Set S1
- Data Set S2
- Data Set S3
- Data Set S4
- Data Set S5
- Data Set S6
- Software S1

Correspondence to:
C. Manning,
cmanning@whoi.edu

Citation:
Manning, C. C., R. H. R. Stanley, D. P. Nicholson, J. M. Smith, J. Timothy Pennington, M. R. Fewings, M. E. Squibb, and F. P. Chavez (2017), Impact of recently upwelled water on productivity investigated using in situ and incubation-based methods in Monterey Bay, *J. Geophys. Res. Oceans*, *122*, 1901–1926, doi:10.1002/2016JC012306.

Received 2 SEP 2016
Accepted 16 JAN 2017
Accepted article online 21 JAN 2017
Published online 11 MAR 2017

Impact of recently upwelled water on productivity investigated using in situ and incubation-based methods in Monterey Bay

Cara C. Manning[1,2,3], Rachel H. R. Stanley[4], David P. Nicholson[2], Jason M. Smith[5], J. Timothy Pennington[6], Melanie R. Fewings[7], Michael E. Squibb[8], and Francisco P. Chavez[6]

[1]MIT/WHOI Joint Program in Oceanography/Applied Ocean Science and Engineering, Woods Hole, Massachusetts, USA, [2]Department of Marine Chemistry and Geochemistry, Woods Hole Oceanographic Institution, Woods Hole, Massachusetts, USA, [3]Department of Earth, Atmospheric and Planetary Sciences, Massachusetts Institute of Technology, Cambridge, Massachusetts, USA, [4]Department of Chemistry, Wellesley College, Wellesley, Massachusetts, USA, [5]Marine Science Institute, University of California, Santa Barbara, California, USA, [6]Monterey Bay Aquarium Research Institute, Moss Landing, California, USA, [7]Department of Marine Sciences, University of Connecticut, Groton, Connecticut, USA, [8]Center for Ocean Solutions, Stanford University, Stanford, California, USA

Abstract Photosynthetic conversion of CO_2 to organic carbon and the transport of this carbon from the surface to the deep ocean is an important regulator of atmospheric CO_2. To understand the controls on carbon fluxes in a productive region impacted by upwelling, we measured biological productivity via multiple methods during a cruise in Monterey Bay, California. We quantified net community production and gross primary production from measurements of O_2/Ar and O_2 triple isotopes ($^{17}\Delta$), respectively. We simultaneously conducted incubations measuring the uptake of ^{14}C, $^{15}NO_3^-$, and $^{15}NH_4^+$, and nitrification, and deployed sediment traps. At the start of the cruise (Phase 1) the carbon cycle was at steady state and the estimated net community production was 35(10) and 35(8) mmol C m^{-2} d^{-1} from O_2/Ar and ^{15}N incubations, respectively, a remarkably good agreement. During Phase 1, net primary production was 96(27) mmol C m^{-2} d^{-1} from C uptake, and gross primary production was 209(17) mmol C m^{-2} d^{-1} from $^{17}\Delta$. Later in the cruise (Phase 2), recently upwelled water with higher nutrient concentrations entered the study area, causing ^{14}C and $^{15}NO_3^-$ uptake to increase substantially. Continuous O_2/Ar measurements revealed submesoscale variability in water mass structure and likely productivity in Phase 2 that was not evident from the incubations. These data demonstrate that O_2/Ar and ^{15}N incubation-based NCP estimates can give equivalent results in an N-limited, coastal system, when the nonsteady state O_2 fluxes are negligible or can be quantified.

1. Introduction

Although microbial carbon uptake in the surface ocean plays a major role in regulating atmospheric CO_2 levels, quantifying the rate of this process has proven challenging on both a local and a global scale [*Emerson*, 2014; *Siegel et al*., 2016]. Through photosynthesis, microbes in the sunlit euphotic zone convert CO_2 to organic carbon (OC), simultaneously consuming nutrients and producing O_2 [*Longhurst and Harrison*, 1989; *Ducklow et al*., 2001]. The majority of the OC is respired back to CO_2 by autotrophs and heterotrophs within the euphotic zone, but some small fraction of the OC is exported to deeper depths in the ocean, where it is isolated from the atmosphere on timescales ranging from weeks to millennia [*Ducklow et al*., 2001; *Emerson*, 2014]. The magnitude of this biological pump and the mechanisms controlling its spatial and temporal variability are thus of great importance for accurately modeling the global carbon cycle and predicting its future changes [*Falkowski et al*., 1998; *Behrenfeld et al*., 2005; *Ciais et al*., 2013].

In this paper, we refer to various aspects of the ecosystem metabolism related to the biological pump [*Williams*, 1993]. *Gross primary production* (GPP) is the total amount of carbon fixed by autotrophic microbes into organic carbon. *Net primary production* (NPP) is GPP minus autotrophic respiration (R_A), i.e., respiration by phytoplankton only. NPP quantifies the amount of carbon available to the heterotrophic community. *Net community production* (NCP) is NPP minus heterotrophic respiration (R_H), or equivalently, GPP minus community respiration (equations (1) and (2)):

$$NPP = GPP - R_A \quad (1)$$

$$NCP = NPP - R_H. \quad (2)$$

NCP quantifies the carbon available for export from the euphotic zone, and therefore NCP is the key parameter in estimating the magnitude of the biological pump [*Laws*, 1991; *Williams and Purdie*, 1991; *Hansell and Carlson*, 1998]. We also use the terms *gross oxygen production* (GOP) to refer to the gross amount of O_2 produced by photosynthesis, and *net oxygen production* (NOP) to refer to the net amount of O_2 produced [*Munro et al*., 2013]. GOP and NOP can be converted to GPP and NCP, respectively, based on empirically derived stoichiometric ratios of O:C for gross and net production [*Laws*, 1991; *Bender et al*., 1999]. In this study, we quantify all five parameters: GPP, NPP, NCP, R_A, and R_H, for the mixed layer, enabling us to estimate the amount of inorganic carbon that is fixed into organic carbon, the amount of organic carbon available for transport out of the mixed layer, and the importance of heterotrophs and autotrophs for recycling carbon within the mixed layer.

Several techniques are available for estimating GPP, NPP, and NCP, including bottle incubations, in situ mass balance techniques, and algorithms derived from satellite-based ocean color data [*Emerson et al*., 1997; *Behrenfeld et al*., 2005; *Emerson*, 2014]. Each method measures a specific aspect of the ecosystem metabolism, integrates over a specific timescale, and is thought to have inherent advantages and disadvantages [*Williams et al*., 2004; *Halsey et al*., 2010; *Juranek and Quay*, 2013; *Emerson*, 2014]. However, very few studies have directly compared incubation and in situ mass balance techniques. There is no single "gold standard" method for measuring productivity, and therefore comparing different methods provides an opportunity to evaluate potential method biases [*Emerson*, 2014; *Siegel et al*., 2016]. Additionally, by measuring different aspects of the ecosystem metabolism at the same time, we gain a fuller understanding of the carbon cycle state (e.g., determining both the rate of export production and the fraction of gross production that is exported), which advances mechanistic understanding of the controls on carbon export. Performing such studies in multiple oceanic environments provides insight into whether the ratio of different parameters (e.g., GPP and NPP) is relatively constant throughout the ocean or varies strongly based on environmental conditions [*Juranek and Quay*, 2013]. These relationships between different productivity parameters and methods could potentially be applied to data sets where fewer productivity methods are used, and could be used to calibrate and improve satellite-based productivity algorithms and ecosystem models [*Siegel et al*., 2016].

Eastern boundary upwelling systems are highly productive and dynamic, and play a large role in the ocean carbon cycle, relative to their small spatial extent [*MacIsaac et al*., 1985; *Falkowski et al*., 1998; *Pennington et al*., 2006]. Specifically, upwelling systems are responsible for ~2% of oceanic primary production, despite occupying just 0.2% of the ocean surface area [*Pauly and Christensen*, 1995]. High productivity at the base of the food web sustains enhanced biomass at higher trophic levels, enabling these regions to support active fisheries [*Peterson et al*., 1988]. In this study, we conducted a research cruise in the Monterey Bay, an embayment on the central California coast, approximately 20 km long and 30 km wide [*Pilskaln et al*., 1996; *Pennington and Chavez*, 2000]. The bay is within an eastern boundary upwelling system (the California Current system) and is affected by wind-driven coastal upwelling, which occurs most intensely just north of the bay at Point Año Nuevo [*Rosenfeld et al*., 1994; *Graham and Largier*, 1997; *Woodson et al*., 2009]. Filaments of cold upwelled water tend to be advected southward from the Point into the middle of the bay, our main study area [*Ryan et al*., 2009]. The large-scale upwelling-favorable winds are most intense in spring and summer but continue periodically into the fall, when this cruise took place [*Graham and Largier*, 1997].

Monterey Bay has been well-studied with respect to biogeochemistry. Monthly, multiyear time series of productivity, based on incubations measuring the uptake of ^{14}C-labeled dissolved inorganic carbon (DIC) and $^{15}NO_3^-$ have been reported previously [*Pennington and Chavez*, 2000; *Wilkerson et al*., 2000], and numerous process-oriented biological studies have been conducted [*Pilskaln et al*., 1996; *Kudela and Dugdale*, 2000; *Ward*, 2005; *Ryan et al*., 2009; *Johnson*, 2010; *Smith et al*., 2014a,2016]. However, productivity estimates derived from in situ measurements of O_2/Ar and the triple oxygen isotopic composition of O_2 have not been published for Monterey Bay.

The in situ O_2 mass balance technique has been widely applied for estimating NCP and GPP in the open ocean [*Juranek and Quay*, 2013], but can be challenging to apply in systems where recently upwelled water is observed at the surface because physically driven O_2 fluxes across the mixed layer can bias estimates of the biological O_2 flux. However, several investigators have recently demonstrated that corrections for entrainment and upwelling can be applied in these systems (e.g., using estimates of the vertical mixing and/or upwelling rates), enabling the determination of productivity from O_2 mass balance in upwelling-influenced systems [*Munro et al*., 2013; *Wurgaft et al*., 2013; *Teeter*, 2014; *Haskell et al*., 2016a]. Furthermore, inferring carbon export below the mixed layer from techniques constrained to the mixed layer is complicated by the fact that lateral transport of surface waters and oceanic fronts may cause a spatial and/or temporal decoupling between carbon fixation and export [*Olivieri and Chavez*, 2000; *Plattner et al*., 2005; *Stukel et al*., 2011; *Estapa et al*., 2015; *Nagai et al*., 2015].

Here we present one of the first published data sets where productivity estimates from both O_2/Ar and the triple oxygen isotope composition of O_2 ($^{17}\Delta$) are combined with multiple other methods including incubations measuring the uptake of ^{14}C, $^{15}NO_3^-$, and $^{15}NH_4^+$ and the nitrification rate (microbial oxidation of NH_4^+ to NO_3^-), as well as sediment trap-based fluxes of particulate carbon and nitrogen (PC and PN). For example, there are few published studies where $^{15}NO_3^-$ uptake (new production) and in situ O_2/Ar (net community production) were measured simultaneously at the same locations [*Emerson et al*., 1993; *Giesbrecht et al*., 2012; *Hamme et al*., 2012]. Although theoretically these two methods should be equivalent at steady state and/or when averaged over large spatiotemporal scales [*Laws*, 1991; *Falkowski et al*., 2003], this assumption has been tested at a limited number of locations, primarily high nitrate, low chlorophyll open ocean regions such as the Southern Ocean and subarctic North Pacific [*Hendricks et al*., 2005; *Reuer et al*., 2007; *Giesbrecht et al*., 2012]. In this study, we estimate GPP, NPP, and NCP by multiple methods in a new environment, a nitrogen-limited, highly productive site [*Kudela and Dugdale*, 2000] within the California Current system. This field-based study enables a more complete understanding of the carbon cycle state than is possible in studies where fewer methods are used.

2. Background on Methods

2.1. ^{14}C Incubations

The ^{14}C-method of estimating primary production (abbreviated herein as ^{14}C-PP) is one of the oldest and most widely used methods of quantifying marine productivity [*Steemann Nielsen*, 1951, 1952], and it is the standard against which many satellite-based productivity algorithms are validated and calibrated [*Behrenfeld and Falkowski*, 1997; *Carr et al*., 2006]. However, there remains uncertainty regarding which aspects of the ecosystem metabolism the incubations measure. The degree to which the incubation captures gross versus net production depends on incubation duration, the time of day at which the incubation is initiated, and even the ratio of photosynthesis to respiration itself [*Steemann Nielsen and Jensen*, 1957; *Williams et al*., 1983; *Williams*, 1993; *Karl et al*., 1996; *Bender et al*., 1999; *Marra*, 2002, 2009; *Pei and Laws*, 2013; *Pennington et al*., 2015]. For example, a 12 h daytime-only incubation will usually yield higher ^{14}C-PP than a 24 h incubation carried out over a full day-night solar cycle, because nighttime respiration will convert some of the OC produced during daytime back to DIC [*Bender et al*., 1999]. Additionally, incubations can be performed on deck (simulating the in situ light levels using screens or other methods) or by suspending the bottles in the water column at the sampling depth. Neither incubation procedure accounts for the natural variability in light experienced by phytoplankton, e.g., as a result of movement within the mixed layer, and the on deck incubations may have additional errors associated with incubation temperature and the spectral quality of the light that passes through the screens [*Grande et al*., 1989; *Marra*, 2002]. Despite these uncertainties, there is generally agreement that 24 h ^{14}C incubations initiated during daytime measure something close to NPP [*Smith et al*., 1984; *Bender et al*., 1999; *Juranek and Quay*, 2005; *Marra*, 2002, 2009; *Juranek and Quay*, 2013].

Another important aspect of the method is that the procedure only measures the carbon that is retained on the filter. The filters retain ^{14}C-POC, and some fraction of the ^{14}C-DOC that is exuded by phytoplankton [*Karl et al*., 1998]. Some of this ^{14}C-DOC is taken up by bacteria which are then retained on the filter. Of the labeled material that remains as DOC when the incubation is terminated, some passes through the filter and some is adsorbed [*Karl et al*., 1998]. The fraction of total OC fixed that is lost as DOC and not retained

on the filter can be up to 30% [*Karl et al*., 1998]. Thus, the incubations underestimate the total ^{14}C uptake into OC. Additionally, the ^{14}C content retained on the filter depends on the filter material (e.g., glass fiber versus polycarbonate). Specifically, glass fiber filters typically retain more DOC than polycarbonate [*Viviani et al*., 2015].

2.2. ^{15}N Incubations

Nitrogen is often a limiting nutrient in marine ecosystems, including Monterey Bay [*Kudela and Dugdale*, 2000]. By measuring uptake of individual N species and nitrification we can better understand the role that nutrient availability plays in regulating primary production.

Phytoplankton assimilate various forms of inorganic nitrogen through processes indirectly related to photosynthesis [*Dugdale and Goering*, 1967]. When these microbes die and/or are eaten, PN, DON, and NH_4^+ (reduced N) are released. Some of the PN sinks below the euphotic zone, and is remineralized to NH_4^+. Over annual timescales, the vast majority of NH_4^+ below the euphotic zone is oxidized to NO_3^- by nitrifying organisms. This NO_3^- is then transferred back to the euphotic zone through upwelling and mixing processes. Within this paradigm, NH_4^+-based production is assumed to approximate regenerated production (as NH_4^+ is produced within the euphotic zone) and NO_3^--based production is assumed to approximate new production (as NO_3^- is produced below the euphotic zone). At steady state, i.e., if the concentration of NO_3^- and organic matter within the euphotic zone is not changing, then new production will equal NCP and export production. If we assume that the only forms of nitrogen taken up by phytoplankton are NO_3^- and NH_4^+, then the sum of the uptake of these two species gives NPP [*Dugdale and Goering*, 1967], after conversion from N to C units based on the Redfield ratio or other C:N data [*Redfield et al*., 1963]. There are, of course, limitations to this approach. The method underestimates the total N uptake because the uptake of other forms of regenerated N such as DON (e.g., urea, amino acids, and proteins) is not quantified [*McCarthy*, 1972; *Eppley and Peterson*, 1979], and because some fraction of the ^{15}N label that is taken up by phytoplankton and then exuded as DON is not retained on the filter. Another important consideration is that nitrification within the euphotic zone can generate a significant fraction of the total euphotic zone NO_3^- inventory in many oceanic regions [*Dore and Karl*, 1996; *Diaz and Raimbault*, 2000; *Yool et al*., 2007; *Grundle et al*., 2013; *Santoro et al*., 2013] including Monterey Bay [*Ward*, 2005; *Smith et al*., 2014a,2014b]. In this study, we performed nitrification rate estimates to separate NO_3^- produced within the euphotic zone from NO_3^- produced below the euphotic zone, for the purpose of calculating new production [*Yool et al*., 2007]. Finally, in some oceanic systems, N_2 fixation is a significant source of new N to the mixed layer. However, N_2 fixation is considered to be negligible in Monterey Bay as the temperature and nutrient conditions are unfavorable to the growth of N_2-fixing organisms [*LaRoche and Breitbarth*, 2005].

An additional methodological challenge is that N occurs at low concentrations in much of the world's oceans [*Moore et al*., 2013], including Monterey Bay [*Kudela and Dugdale*, 2000], and therefore the addition of bioavailable nitrogen could perturb nutrient cycling within the incubation bottle. Ideally, the concentration of tracer added should be $\leq$10% of the ambient concentration to ensure that the tracer itself does not stimulate N assimilation and primary production [*Dugdale and Goering*, 1967].

2.3. O_2 Mass Balance

Measurements of O_2/Ar gas ratios and the triple oxygen isotopic composition of O_2 are effective tracers of NCP and GPP, respectively. The O_2/Ar mass balance technique has become a widely used approach for in situ determinations of NCP. Both gases have similar diffusivity, solubility, and dependence of solubility on temperature [*Ferrell and Himmelblau*, 1967; *Jähne et al*., 1987; *Garcia and Gordon*, 1992; *Hamme and Emerson*, 2004]. As a result, Ar is commonly used as an abiotic analogue for O_2; Ar responds similarly to physical forcings but has no biological flux [*Craig and Hayward*, 1987; *Spitzer and Jenkins*, 1989]. To calculate net biological production of O_2, investigators must correct for the effect of physical processes because in many environments the physical and biological fluxes of O_2 are similar in magnitude in the mixed layer [*Emerson*, 1987; *Hamme and Emerson*, 2006; *Castro-Morales and Kaiser*, 2012; *Giesbrecht et al*., 2012]. Physical processes that affect O_2 include air-sea gas exchange, vertical mixing/entrainment, and lateral advection.

The triple oxygen isotopic tracer of dissolved O_2 exploits the unique isotopic signatures of O_2 produced by photosynthesis, consumed by respiration, and added to the ocean by air-sea gas exchange [*Luz and Barkan*, 2000, 2005; *Juranek and Quay*, 2013]. Specifically, photochemical reactions in the upper atmosphere impart

a small mass-independent isotopic fractionation signature on tropospheric O_2, which is transferred to O_2 dissolved in the ocean through air-sea gas exchange [*Thiemens et al*., 1995; *Luz and Barkan*, 2000], with a known mass-dependent fractionation [*Reuer et al*., 2007; *Stanley et al*., 2010]. Photosynthetic O_2 is derived from H_2O, which does not have a measurable mass-independent isotopic signature [*Luz and Barkan*, 2000; *Juranek and Quay*, 2013]. Respiratory isotopic fractionation of O_2 has been determined experimentally [*Luz and Barkan*, 2005].

In many studies, each location is only sampled once (e.g., transect cruises) or sampling at the same location occurs very far apart in time (much longer than the residence time of O_2 in the mixed layer, which is typically on the order of 2 weeks), making it necessary to assume the gases are at steady state in order to calculate NCP and GPP [*Stanley et al*., 2010; *Giesbrecht et al*., 2012; *Munro et al*., 2013]. When a higher-frequency time series of measurements is obtained (as occurred during this cruise), investigators can quantify the change in $[O_2]$ and $^{17}\Delta$ with time and include these terms in the productivity estimates when appropriate [*Hamme et al*., 2012; *Tortell et al*., 2014; *Wilson et al*., 2015]. Because the calculations of NCP and GPP from O_2/Ar and triple oxygen isotope data can vary substantially between studies, we outline our calculations in section 4.

2.4. Sediment Traps

Sediment traps directly measure the flux of organic particles out of the surface ocean, in contrast to the previously described methods which measure processes within the surface ocean and are used to infer downward organic matter flux [*Buesseler*, 1991; *Emerson*, 2014]. To interpret the sediment trap data, we must keep in mind that there are three main modes of OC export: passive sinking of particles, active transport by zooplankton and other animals who consume OC near the surface and exude it at depth, and physical transport of OC by mixing and advection [*Buesseler*, 1991; *Carlson et al*., 1994; *Steinberg et al*., 2000; *Emerson*, 2014]. Sediment traps primarily capture the passively sinking particulate flux. Of the met6 hods used during this cruise, sediment traps are the only one that measures any component of the export flux directly, and the only one that quantifies a flux below the euphotic zone.

A challenge in the use and interpretation of data from upper ocean particle traps, which are intended to collect the passively sinking flux of detrital matter, is the inadvertent collection of actively swimming zooplankton in the trap [*Michaels et al*., 1990]. These living organisms can be a significant portion of the carbon content retained on the filter but do not represent carbon export. Various correction methods for zooplankton swimmers can be used, including placing screens within the particle traps to prevent zooplankton from sinking to the bottom, counting zooplankton within the unfiltered trap water and/or manually removing zooplankton from the filter paper after filtration [*Michaels et al*., 1990].

3. Field and Analytical Methods

3.1. Cruise Description

The cruise (CANON14) took place from 27 September to 3 October 2014. During the cruise, we obtained casts with a conductivity-temperature-depth sensor (CTD, Sea-Bird SBE 9) and Niskin bottle rosette to ~180 m four times per day, at roughly 06:00, 12:00, 18:00, and 00:00 local time. Throughout the paper, all dates and times are reported as local time (UTC − 07:00). All CTD casts at 6 h intervals were obtained near mooring 1 (M1, 36.75°N, 122.03°W, 21 km west of Moss Landing, CA), which is operated by the Monterey Bay Aquarium Research Institute. Sunrise and sunset were at 07:00 and 19:00, respectively. Immediately prior to nearly every cast, we obtained vertical profiles of microscale turbulence to ~70 m using a vertical microstructure profiler (VMP-200, Rockland Scientific). Rates of turbulent kinetic energy dissipation were calculated using the profiler's shear probes and fast temperature sensor, and diapycnal dissipation and diffusivity (K_z) were estimated following *Wolk et al*. [2002]. These diffusivity measurements are used to quantify the impact of vertical mixing on the mass balance of the gas tracers [*Manning et al*., 2016a].

Throughout the cruise, an autonomous underwater vehicle (AUV) drifted at $\sigma_\theta \approx 25.2$ kg m^{-3} (25–45 m depth), near the base of the thermocline. We conducted CTD casts and deployed sediment traps (section 3.5) in the vicinity of the drifting subsurface AUV; however, the ship's course between casts sometimes varied in order to meet other science goals (supporting information Figures S1 and S2). We use wind speed measurements obtained by a Vaisala ultrasonic anemometer from M1 to calculate air-sea gas transfer coefficients (k, section 4.1).

3.2. Rates of ^{14}C Uptake (^{14}C-PP)

We collected water for incubation-based measurements of ^{14}C-PP just prior to dawn each day from depths corresponding to 100, 50, 30, 15, 5, 1, and 0.1% I_o, where I_o is the photosynthetically active radiation (PAR) at the sea surface (0 m depth), estimated using a Secchi disk. Upon return to deck, we drained water from each depth into clear, acid cleaned, 1 L polycarbonate bottles and added $^{14}C-HCO_3^-$ to each bottle following [*Pennington et al*., 2015]. We loaded the incubation bottles into bags made of neutral density screen, layered to attenuate surface irradiance to the appropriate in situ light levels and then placed all samples in an on deck incubator cooled with ambient surface (~2 m) seawater (temperature range: 15.1–16.8°C). After 24 h, we terminated the incubations by filtration and analyzed the filters for ^{14}C following [*Pennington et al*., 2015].

To determine the depth-integrated ^{14}C-PP (estimated using trapezoidal integration), we first estimate the euphotic zone depth using the depth-integrated chlorophyllous pigment content in the water column and equation ((1)a) of *Morel and Berthon* [1989]. Then the simulated depth of each incubation (e.g., the depth equivalent to 30% I_o) is estimated using the Beer-Lambert Law, $I_z/I_o = \exp(-kz)$, with k the extinction coefficient calculated from the euphotic zone depth (the depth, z, where $I_z/I_o = 0.01$).

Each daily ^{14}C-PP measurement has an error of ±7% RSD (relative standard deviation), based on another data set of triplicate incubations by the authors [*Pennington et al*., 2015]. During this cruise, a single incubation was carried out at each depth.

3.3. Rates of $^{15}NO_3^-$ Uptake, $^{15}NH_4^+$ Uptake, and Nitrification

As for the ^{14}C-PP incubations, we collected water for incubation-based measurements of $^{15}NO_3^-$ uptake, $^{15}NH_4^+$ uptake, and nitrification just before dawn each day from depths of 50, 30, 15, 5, 1, and 0.1% I_o. We followed the procedures of *Kudela and Dugdale* [2000] and *Smith et al*. [2014b] for the incubations. As for the ^{14}C incubations, the incubations occurred on deck using neutral density screen to simulate the in situ light levels. Two sets of incubations took place: one set included all light depths and was held for 24 h; a second set from 50%, 1%, and 0.1% light were terminated after 6 h to assess the effects of incubation time and isotope dilution on rate estimates. We added isotopically labeled substrates to a final concentration of 0.2–1 μmol L^{-1} of $^{15}NO_3^-$ and 0.08 μmol L^{-1} of $^{15}NH_4^+$. For NO_3^-, we targeted a 10% ^{15}N enrichment at the start of each incubation using an established relationship between temperature and [NO_3^-] in Monterey Bay because nutrient analyses were not yet available at the time of incubation. For NH_4^+, we added a fixed quantity of tracer to all bottles, which was selected to ensure ^{15}N uptake was detectable, while also minimizing perturbation to the system over the 3 orders of magnitude range in [NH_4^+] observed in Monterey Bay and the contiguous California Current system [*Smith et al*., 2014a,2016]. Postcruise analysis indicates that average ^{15}N tracer additions represented 51(8)% and 208(31)% of the ambient NO_3^- and NH_4^+ pools, respectively. The predicted nutrient concentrations were an overestimate, in part due to the anomalously warm and nutrient-poor surface water mass that persisted in the region during our cruise [*Bond et al*., 2015; *Seager et al*., 2015]. The potential biases that could result from the non-negligible tracer enrichments are discussed in section 5.3.

Analyses of PN concentration and isotopic ratios occurred at the University of California, Santa Barbara Marine Science Institute. Measurement of ^{15}N in the $NO_3^-+NO_2^-$ pool occurred at the University of Connecticut in the Granger Lab by the denitrifier method [*Sigman et al*., 2001]. Reference materials USGS32, USGS34, and USGS35 were analyzed in parallel to calibrate δ^{15}N values.

We calculated ^{15}N uptake and nitrification in each incubation bottle following *Dugdale and Goering* [1967] and adjusted the NH_4^+ uptake and nitrification rates for isotope dilution following *Kanda et al*. [1987], by comparing the uptake estimates from the 6 and 24 h incubations. Isotope dilution corrections increased NH_4^+ uptake by 30%, and increased nitrification rates by 400%. Even with the revised, higher nitrification rate estimates, mixed layer nitrification rates were only 2% of NO_3^- uptake.

We calculated the depth-integrated ^{15}N uptake and nitrification rates using a trapezoidal integration based on the depth at which each Niskin bottle was closed (rather than the light-equivalent depth) because the uptake rates are calculated with respect to the nutrient concentrations measured in the bottle. Since incubations were not performed at 100% I_o, we assumed the ^{15}N uptake at 100% I_o (0 m depth) is equivalent to the uptake at 50% I_o (~2 m depth). Nitrate uptake rates integrated to the base of the euphotic zone (1% I_o)

were on average 1.3 times the rates integrated to 14 m (range 1.2–1.5 times). Ammonium uptake rates integrated to the base of the euphotic zone were on average 2.7 times the rates integrated to the mixed layer depth (5.6 times for the first injection and 1.6–2.4 times for the other four). Nitrification rates integrated to the depth of the euphotic zone were on average 23 times the mixed layer integrated rates (87 times for the first incubation and 3.4 to 10.1 for the other four), and euphotic zone nitrification rates were 10% or less of the euphotic zone nitrate uptake rates.

We estimate the error of each daily incubation measurement to be ±9% for NO_3^- uptake, ±23% for NH_4^+ uptake, and ±15% for nitrification. These estimates are based on the reproducibility (standard deviation) of prior duplicate incubations of mixed layer water in Monterey Bay (unpublished results from coauthor Jason Smith). During this cruise, a single incubation was carried out at each depth.

3.4. $[O_2]$, [Ar], O_2/Ar, and $^{17}\Delta$ Analysis

Throughout the cruise, we measured O_2 and Ar concentrations ($[O_2]$ and [Ar]), O_2/Ar mole ratios ($n(O_2)/n(Ar)$, abbreviated herein as O_2/Ar), and the triple oxygen isotopic composition of O_2 ($\delta^{17}O$, $\delta^{18}O$, and $^{17}\Delta$).

We used a field-deployable mass spectrometer (gas equilibration mass spectrometer, GEMS) to measure O_2/Ar near-continuously from the underway system (2 m depth). We configured the instrument as described in *Manning et al.* [2016b], except that we removed the getter chamber (a purification chamber that removes all of the non-noble gases) and the mass spectrometer was a Pfeiffer PrismaPlus QMG200. The system is similar to the equilibrator inlet mass spectrometer developed by *Cassar et al.* [2009]. For calibration, the system measured O_2/Ar in air for 40 min after every ~4 h of sampling the headspace of the equilibrator cartridge. We manually controlled the exact switching times to ensure that we obtained data while on station for the CTD casts whenever possible.

We analyzed 154 discrete samples from either the underway seawater system or from Niskin bottles for O_2/Ar, $\delta^{17}O$, and $\delta^{18}O$ with a Thermo Fisher Scientific MAT 253 isotope ratio mass spectrometer at the Woods Hole Oceanographic Institution. We followed the protocol of *Barkan and Luz* [2003] with some modifications [*Stanley et al.*, 2010, 2015]. We analyzed samples 4–7 months after the evacuation of the flasks (3–5 months after sampling). The precision (mean standard deviation) of replicate field samples from the same Niskin bottle was 5.0 per meg for $^{17}\Delta$, 0.015‰ for $\delta^{17}O$, 0.031‰ for $\delta^{18}O$, and 0.12% for $\Delta(O_2/Ar)$. For samples from the underway seawater line collected in rapid succession (within 8 min), the precision was 6.7 per meg for $^{17}\Delta$, 0.023‰ for $\delta^{17}O$, 0.047‰ for $\delta^{18}O$, and 0.38% for $\Delta(O_2/Ar)$, and this lower precision is likely related to real environmental variability that is not captured in samples collected from the same Niskin bottle. See section 4.2 for more details on the triple oxygen isotope terminology.

On the day before the cruise departed, we flushed the underway line with bleach to remove biofilms that could cause high rates of respiratory consumption of O_2 [*Juranek et al.*, 2010]. After the cruise, we evaluated the agreement between the different sampling and analytical methods. Using all discrete near-surface samples (underway and Niskin), the average difference between the discrete samples and the GEMS was −0.05(1.11)%. Furthermore, the mean offset between the surface Niskin samples and the underway GEMS was 0.14(1.22)%. We did not apply any correction to the GEMS data because these mean offsets were very small relative to the uncertainty in the offset.

We obtained measurements of $[O_2]$ using a SBE 43 sensor on the CTD rosette and calibrated the sensor via Winkler titration [*Carpenter*, 1965]. Using 25 water samples collected throughout the cruise and analyzed at sea, we applied a single calibration to all O_2 data: $[O_2]_{cal} = 1.0075[O_2]_{meas} + 2.87$ ($R^2 = 0.9993$) with $[O_2]_{cal}$ and $[O_2]_{meas}$ the calibrated and measured (uncalibrated) concentrations in μmol kg^{-1}.

We also collected discrete samples for measurement of noble gas concentrations (He, Ne, Ar, Kr, and Xe). Briefly, water samples were collected in copper tubes and sealed with a cold pressure welder; gas was subsequently extracted from the water and analyzed using a quadrupole mass spectrometer [*Stanley et al.*, 2009; *Loose et al.*, 2016]. In this paper, we only use the [Ar] results, which had an estimated error (combined precision and accuracy) of 0.24% RSD (relative standard deviation). See *Manning et al.* [2016a] for the complete noble gas data.

3.5. Sediment Trap-Based Particle Fluxes

We deployed shallow particle interceptor traps (PITS) composed of three individual plastic collection tubes, each 1.4 L in volume [*Knauer et al.*, 1979] at 50 m depth, connected to a surface drifter. We filled the traps with 0.2 μm filtered seawater prior to deployment and added two 10 g NaCl pills to the base of each tube to form a dense brine to retain the particulate material. Deployments lasted ∼24 h, beginning daily between dawn and noon. Once on deck, using 0.2 μm filtered seawater, we emptied each collection tube, rinsed three times, and made each sample up to 2.0 L. Then we filtered 0.5 L from each 2.0 L sample and froze the filters for subsequent analysis for POC and PN content at the University of California Santa Barbara Marine Science Institute by online combustion [*Hedges and Stern*, 1984]. For five of the six deployments, we removed another 33 mL from each sample and then combined the three fractions and analyzed the samples by microscopy for quantitative taxonomic identification of zooplankton swimmers. We used this data to estimate the zooplankton volume and carbon content [*Nozais et al.*, 2005]. Estimates of the swimmer C flux from individual traps ranged from 8% to 65% of the total POC flux from the same trap.

3.6. Nutrients and Pigments

We analyzed concentrations of phaeopigments and chlorophyll by filtering water samples onto glass fiber filters (GF/F), extracting pigments with acetone, and analyzing with a Turner fluorometer [*Pennington and Chavez*, 2000]. We measured ammonium concentration on fresh unfiltered seawater samples immediately after collection using a fluorimetric method [*Holmes et al.*, 1999], and for all other nutrients, we froze unfiltered samples aboard ship [*Dore and Karl*, 1996] for later analysis with an Alpkem 300 autoanalyzer [*Sakamoto et al.*, 1990]. Detection limits were 0.5, 0.5, and 0.01 μmol kg^{-1} for SiO_4, NO_3^-, and NH_4^+, respectively, and error was ∼ 0.6%, 3%, and 0.5% at maximum range for SiO_4, NO_3^-, and NH_4^+.

3.7. Satellite Data

We used satellite-based sea surface temperature (SST) maps from MODIS Aqua and Terra [*JPL/OBPG/RSMAS*, 2006a,2006b] to assess the spatial structure of near-surface temperature within the bay. To determine whether the satellite data were contaminated by cloud cover, we examined true-color satellite images, which showed that 25–26 September and 30 September to 3 October were nearly cloud-free within Monterey Bay whereas 27–29 September had significant clouds within the bay. We included SST pixels with a quality level of 2 or higher (level 5 is the highest quality), and eliminated the most questionable data (level 1). Many of the pixels masked at quality levels 2–4, predominantly in relatively small areas to the north and south of Monterey Bay near the coast, persisted in the same locations and shapes in multiple images separated by many hours or days. This indicates those temperature features were likely real oceanographic features (SST fronts and cold filaments) rather than clouds. Incorrect flagging of strong SST fronts as clouds is a known issue in the MODIS quality algorithms in coastal regions [*Oram et al.*, 2008; *Nieto et al.*, 2012]. SST data within the main study area are not sensitive to the choice of quality level.

4. Calculations

4.1. Calculation of NOP From O_2/Ar Mass Balance

We quantify the biologically generated supersaturation (or undersaturation) of O_2 with respect to Ar using the tracer $\Delta(O_2/Ar)$:

$$\Delta(O_2/Ar) = \left[\frac{(O_2/Ar)}{(O_2/Ar)_{eq}} - 1\right]. \quad (3)$$

Here (O_2/Ar) and $(O_2/Ar)_{eq}$ are the measured and equilibrium mole ratios, respectively, and $\Delta(O_2/Ar)$ is often expressed in percent by multiplying by 100%. ΔO_2 is defined similarly, by removing Ar from equation (3). We calculate the gas saturation states using the solubility data of *Hamme and Emerson* [2004] for Ar and *Garcia and Gordon* [1992] for O_2. For the gas diffusivity, we use the data of *Ferrell and Himmelblau* [1967] for O_2 and extrapolated values for Ar based on the data for other noble gases in *Jähne et al.* [1987]; *Manning and Nicholson* [2016].

Net O_2 production (NOP) measures the net autotrophic production of O_2 minus community respiratory consumption by autotrophs and heterotrophs. We define the biological O_2, $[O_2]_B$ as

$$[O_2]_B = \Delta(O_2/Ar)[O_2]_{eq}\frac{[Ar]}{[Ar]_{eq}} = [O_2] - [O_2]_{eq}\frac{[Ar]}{[Ar]_{eq}}. \quad (4)$$

We include the term $[Ar]/[Ar]_{eq}$, in contrast to other studies where it is often assumed that $[Ar]/[Ar]_{eq} = 1$ if [Ar] is not directly measured [*Hamme and Emerson*, 2006; *Stanley et al*., 2010; *Giesbrecht et al*., 2012]. Our discrete Ar samples indicate that $[Ar]/[Ar]_{eq} = 1.036(0.006)$ within the mixed layer and displayed no consistent gradients with depth or time [*Manning et al*., 2016a]; we used this average value to calculate $[O_2]_B$ throughout the cruise, which increases $[O_2]_B$ by 3.6%, compared to assuming $[Ar]/[Ar]_{eq} = 1$.

We calculate the mixed layer NOP as the rate of biological O_2 production equalling the loss of biological O_2 to gas exchange and vertical mixing, and the rate of change in biological O_2 with time [*Cassar et al*., 2011; *Hamme et al*., 2012; *Cassar et al*., 2014]

$$NOP = k_{O_{2,w}}[O_2]_B + K_z\frac{\partial[O_2]_B}{\partial z} + h\frac{\partial[O_2]_B}{\partial t}, \quad (5)$$

where $k_{O_{2,w}}$ is the time-weighted gas transfer velocity for O_2 (m d^{-1}), calculated using the algorithm of *Reuer et al*. [2007] with the wind speed-based parameterization of *Sweeney et al*. [2007], K_z is the vertical diffusivity (m^2 d^{-1}) from microstructure profiles, and h is the mixed layer depth (m). The terms $\partial[O_2]_B/\partial t$ and $\partial[O_2]_B/\partial t$ refer to the rate of change of $[O_2]_B$ with depth and time, respectively.

At steady state, i.e., if there is no change in $[O_2]_B$ with time, then equation (5) simplifies to

$$NOP = k_{O_{2,w}}[O_2]_B + K_z\frac{\partial[O_2]_B}{\partial z}. \quad (6)$$

A time series of O_2 is needed to estimate $\partial[O_2]_B/\partial t$. However, in many studies, a time series is not available and it is necessary to assume $\partial[O_2]_B/\partial t = 0$ and use the steady state equation in order to estimate NOP from O_2 measurements [*Juranek and Quay*, 2013]. In this study, we have a time series and are able to assess whether equation (5) or (6) is more appropriate.

In equations (5) and (6), the term $k_{O_{2,w}}$ is calculated using wind speed measured at M1. During the entire cruise $k_{O_{2,w}} = 1.79(0.07)$ m d^{-1}. We omit lateral advection from the mass balance because we did not observe consistent gradients in $[O_2]_B$ in the mixed layer between our main sampling area (within 5 km of the mean cast location) and the water outside this area (supporting information Figures S1 and S2). We calculate $[O_2]_B$ over the mixed layer, which is shallower than the euphotic zone depth (1% I_o), because we have continuous O_2/Ar measurements at the surface only and because the subsurface physical fluxes of O_2 are more difficult to quantify because they are due to mixing and transport, rather than air-sea exchange. Using the CTD $[O_2]$ profiles every 6 h and/or the O_2/Ar profiles measured more sporadically, we could not distinguish the small subsurface $[O_2]_B$ fluxes from the large fluxes due to physical processes such as internal waves and lateral advection.

In this study, we used K_z profiles obtained during the cruise to parameterize the vertical flux of $[O_2]_B$ out of the mixed layer. In many other studies, K_z is estimated based on past measurements, which can induce a factor of 10 uncertainty into the vertical O_2 flux, and is sometimes the largest source of error in estimates of NOP [*Hamme and Emerson*, 2006; *Giesbrecht et al*., 2012; *Jonsson et al*., 2013; *Cassar et al*., 2014; *Weeding and Trull*, 2014]. For each CTD cast that was immediately preceded by microstructure profiles, we calculated the vertical biological O_2 gradient, $\partial[O_2]_B/\partial z$ from a linear regression of the measured $[O_2]_B$ profile from the base of the mixed layer to 10 m below the mixed layer (Figure 1b). We multiplied this vertical gradient by K_z at the mixed layer depth, linearly interpolated to the same time as the CTD cast (Figure 1a). The average K_z at the base of the mixed layer was $1.6(2.4) \times 10^{-5}$ m^2 s^{-1} and the range was 9.5×10^{-7}–1.1×10^{-4} m^2 s^{-1}. This result is similar to estimates by *Haskell et al*. [2016b] who determined $K_z = 1.5(0.6) \times 10^{-5}$ m^2 s^{-1} at the base of the mixed layer during fall and winter in the Southern California Bight, using a wind speed-based parameterization of turbulence due to shear [*Haskell et al*., 2016a]. The average vertical biological O_2 flux was $-3.5(4.6)$ mmol O_2 m^{-2} d^{-1}, and the range was -19.0 to -0.1 mmol O_2 m^{-2} d^{-1}. One cast yielded a much larger magnitude flux of -95 mmol O_2 m^{-2} d^{-1}; this cast was not included in the average K_z and O_2 fluxes because it was an outlier. Due to the wide range in O_2 fluxes estimated from individual profiles, and the lack of consistent changes with time, we applied the average vertical biological O_2 flux to all casts. Vertical mixing increased the calculated NOP by less than 10%, and constraining this flux reduces uncertainty in our NOP calculations.

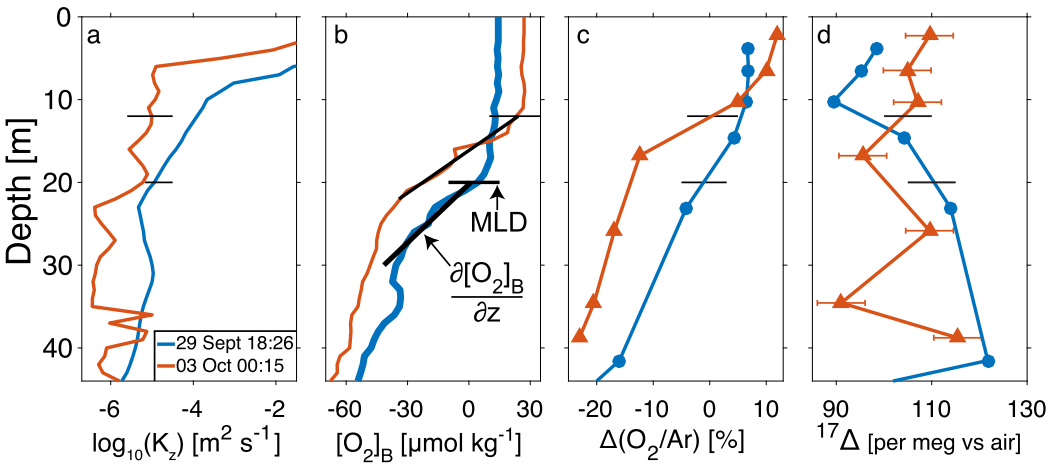

Figure 1. Representative profiles of (a) K_z, (b) O_2, (c) $\Delta(O_2/Ar)$, and (d) $^{17}\Delta$ ($\lambda = 0.5179$). Black horizontal lines on Figures 1a–1d indicate mixed layer depth, and black slopes in Figure 1b show the vertical gradient in O_2. In Figure 1c, measurement error is smaller than filled symbols, and in Figure 1d, representative measurement error is shown on one profile with error bars.

For each cast, we define the O_2-based mixed layer depth (MLD) as the first depth below 10 m where $[O_2]$ is more than 1% different from the value at 10 m, similar to *Castro-Morales and Kaiser* [2012]. The MLD averaged 14(4) m and we used this average MLD of 14 m as the integration depth when calculating mixed layer productivity from the incubations (sections 5.2–5.3).

We convert NOP to NCP (from oxygen units to carbon units) using an O_2:C ratio (photosynthetic quotient, PQ) of 1.4 and 1.1 for NO_3^- and NH_4^+ driven uptake, respectively [*Laws*, 1991]. The O_2:C photosynthetic quotient was 1.33 in Phase 1 and 1.35 in Phase 2, based on the mixed layer NO_3^- and NH_4^+ uptake incubations (section 5.3).

4.2. Calculation of GOP From $^{17}\Delta$

Using the triple isotopic composition of O_2 we can estimate the rate of GOP. We characterize the isotopic composition of O_2 using the tracers $\delta^{18}O$, $\delta^{17}O$, and $^{17}\Delta$. We define $\delta^{18}O = X^{18}/X^{18}_{air} - 1$. Here $X^{18} = r(^{18}O/^{16}O)$ is the measured ratio and $X^{18}_{air} = r(^{18}O/^{16}O)_{air}$ is the ratio of O_2 in air, collected locally, which we used as the reference standard. The tracer $\delta^{17}O$ is calculated analogously. The terms $\delta^{18}O$ and $\delta^{17}O$ are often expressed in ‰ by multiplying by 1000.

We define $^{17}\Delta$ as

$$^{17}\Delta = \ln(\delta^{17}O + 1) - \lambda \ln(\delta^{18}O + 1). \quad (7)$$

Here we use $\lambda = 0.5179$ which is the empirically determined ratio of the fractionation factors for respiratory O_2 consumption in ^{17}O relative to ^{18}O (i.e., $\lambda = {}^{17}\epsilon/{}^{18}\epsilon$) [*Luz and Barkan*, 2005]. Using this definition, $^{17}\Delta$ is not changed by respiration but is affected by photosynthesis, air-sea gas exchange, and mixing between water masses [*Hendricks et al.*, 2005; *Juranek and Quay*, 2013; *Nicholson et al.*, 2014]. For dissolved O_2 in water, $^{17}\Delta$ is typically reported in per meg (1 per meg = 0.001‰) due to the small range of values. O_2 derived from air-sea equilibrium has $^{17}\Delta \simeq 8$ per meg [*Reuer et al.*, 2007; *Stanley et al.*, 2010], and O_2 that is purely biological in origin has $^{17}\Delta \simeq 293$ per meg with $\lambda = 0.5179$. Thus $^{17}\Delta$ is a tracer of the proportion of O_2 in a given water parcel that was generated from biological activities, relative to the amount added via air-sea exchange.

The most accurate method of calculating GOP from the triple oxygen isotopic composition of O_2 has received much discussion in the literature. There is currently no single universally accepted method of calculating GOP, and many authors have argued that the ideal choice of parameters and constants may depend on properties of the system (e.g., the microbial species of interest and isotopic composition of oxygen in water, which is the source of photosynthetic O_2) [*Luz and Barkan*, 2000; *Juranek and Quay*, 2005; *Reuer et al.*, 2007; *Luz and Barkan*, 2009; *Stanley et al.*, 2010; *Kaiser*, 2011; *Luz and Barkan*, 2011; *Nicholson et al.*, 2011; *Prokopenko et al.*, 2011; *Hamme et al.*, 2012]. However, there is strong scientific consensus that

calculations should be performed using the individual isotope ratios rather than the empirically defined term $^{17}\Delta$ which is a combination of two isotope ratios [*Kaiser*, 2011; *Luz and Barkan*, 2011; *Nicholson et al*., 2011; *Prokopenko et al*., 2011]. We include the raw data ($\delta^{17}O$, $\delta^{18}O$, $^{17}\Delta$, $\Delta(O_2/Ar)$, $[O_2]$, salinity, temperature, depth, and wind speed) as a supplement to this paper (data set 2) so that GOP can be recalculated in the future using new formulas [*Kaiser*, 2011]. We also provide the MATLAB code used to calculate GOP in supporting information and on GitHub (http://github.com/caramanning/calcGOP), to ensure that the calculations in this paper can be reproduced by others.

We use the following equation to calculate GOP (equation (S8) from *Prokopenko et al*. [2011]):

$$GOP = \frac{k[O_2]_{eq}\left[\frac{X^{17}-X^{17}_{eq}}{X^{17}} - \lambda\frac{X^{18}-X^{18}_{eq}}{X^{18}}\right] + h[O_2]\frac{\partial^{17}\Delta}{\partial t}}{\left[\frac{X^{17}_p-X^{17}}{X^{17}} - \lambda\frac{X^{18}_p-X^{18}}{X^{18}}\right]}. \quad (8)$$

Here h is the mixed layer depth, k is the gas transfer velocity for O_2, $X^{17} = r(^{17}O/^{16}O)$ and the subscripts p and eq refer to O_2 produced by photosynthesis and at air-sea equilibrium, respectively, and $\lambda = 0.5179$ as in equation (7). Oxygen terms without a subscript ($[O_2]$, X^{17}, and $^{17}\Delta$) are the measured mixed layer values. At steady state, i.e., if there is no change in $^{17}\Delta$ with time, then $h[O_2]\partial^{17}\Delta/\partial t = 0$, and equation (8) simplifies to equation (7) of *Prokopenko et al*. [2011].

We calculate X^{18}_{eq} based on *Benson and Krause* [1984] and *Benson and Krause* [1980], and X^{17}_{eq} from *Stanley et al*. [2010] ($^{17}\Delta_{eq} = 8$ per meg, which is consistent with our daily analyses of equilibrated water at room temperature). We assume that the seawater (the substrate for photosynthetic O_2) has the isotopic composition of VSMOW, as defined with respect to air in *Barkan and Luz* [2011], and that photosynthetic O_2 has the isotopic composition of average phytoplankton defined in *Luz and Barkan* [2011]. If we instead assume that the surface seawater in Monterey Bay has an isotopic composition of $\delta^{18}O = -0.5761$ and $\delta^{17}O = -0.3092‰$ with respect to VSMOW, based on a global gridded data set of $\delta^{18}O$ in seawater [*LeGrande and Schmidt*, 2006] and published relationships between $\delta^{17}O$ and $\delta^{17}O$ in seawater [*Luz and Barkan*, 2010], GOP is ~11% higher. Since we did not collect water samples for measurement of the isotopic composition, and the global data set may be less accurate in coastal regions, we felt it was more appropriate to use the composition of VSMOW.

We omit the terms for kinetic isotopic fractionation during air-sea gas exchange in equation (8), which have been included in some other studies [*Kaiser*, 2011; *Nicholson et al*., 2011; *Hamme et al*., 2012; *Nicholson et al*., 2014]. Including these terms decreases GOP by 1%, which is well within the error of the method. In regions with higher wind speeds, this term will become more important. Also, we do not include a correction for vertical mixing/entrainment of O_2 [*Nicholson et al*., 2012; *Wurgaft et al*., 2013; *Nicholson et al*., 2014] because we found that there was no consistent gradient in $^{17}\Delta$ with depth below the mixed layer (Figure 1d).

Given that we did not observe a trend in $^{17}\Delta$ with time, we calculated steady state GOP for each individual sample, then bin-averaged the samples using a 2 h window. This approach helped to ensure that times when sampling frequency was higher and replicates were analyzed were not over-weighted when calculating the average GOP.

The conversion of GOP (in mol O_2 m^{-2} d^{-1}) to GPP (in mol C m^{-2} d^{-1}) requires the correction for light-dependent respiration processes that consume photosynthetically generated O_2 but do not fix C. We estimate $GPP = (GOP - 0.19GOP)/PQ$ where the PQ (photosynthetic quotient) is 1.33 in Phase 1 and 1.35 in Phase 2, the PQ used for the conversion of NOP to NCP. The value of 0.19 is the fraction of GOP associated with light-dependent respiration determined in culture studies by *Halsey et al*. [2010] and falls within the 10–30% range reported in several other studies [*Kana*, 1992; *Bender et al*., 1999; *Laws et al*., 2000; *Juranek and Quay*, 2013].

5. Results and Discussion

5.1. Hydrographic and Biogeochemical Setting

For this study, we consider all CTD/Niskin bottle data, all sediment trap data, and all underway data collected within a 5 km radius of the mean CTD profile location (Figure 2). The mean location is a central point where the average distance to all 23 CTD casts is minimized. The 5 km radius is the minimum distance that included all CTD cast locations. If we had included all underway measurements (supporting information

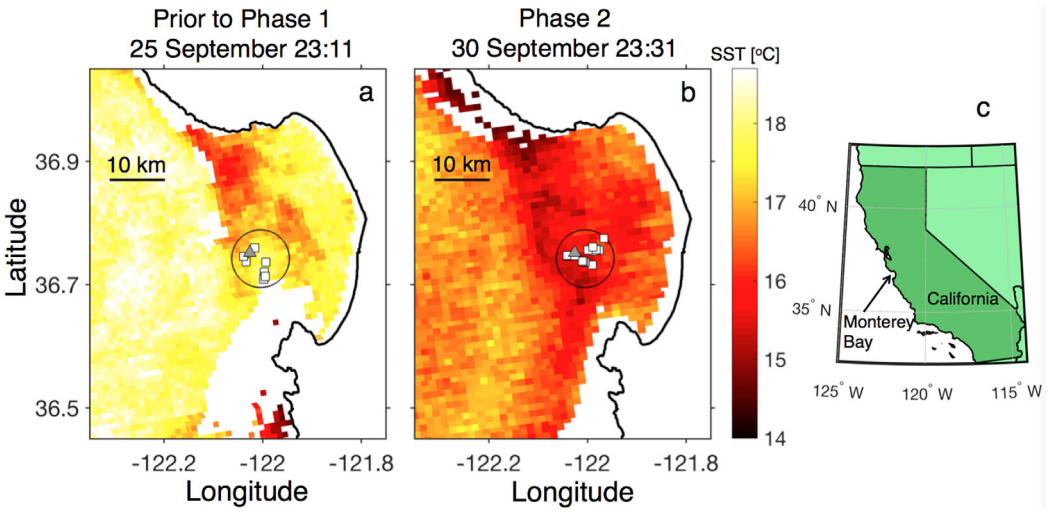

Figure 2. Map of study site showing MODIS sea surface temperature measured (a) 25 September 23:11 (prior to Phase 1) and (b) 30 September 23:31 (during Phase 2). White areas over water indicate that no satellite SST data were available. White squares show locations of CTD casts in Phase 1 (a) and Phase 2 (b). Grey triangles show location of mooring M1. The black circle shows the region within 5 km of the mean profile. (c) Map of California showing location of Monterey Bay.

Figure S1 in our productivity estimates from O_2, this could have generated more biases between the incubation/trap and O_2 measurements due to the significant spatial variability in physical properties and productivity within Monterey Bay and contiguous waters that is recorded in the underway record but not the other methods [*Pennington and Chavez*, 2000; *Ryan et al.*, 2009]. Throughout the paper, all results are expressed as mean($\pm$ standard deviation) unless otherwise specified.

We separate the cruise into two phases, based on the surface water characteristics (Figures 2–4). Phase 1 is a relatively stable period beginning with the first CTD cast on 27 September 15:00 and ending 29 September 09:35. Phase 2 is a more dynamic period beginning 29 September 09:35 and lasting through the end of the cruise, during which we sampled multiple water masses at the surface, including a colder, recently upwelled filament, as well as a warmer water mass in which the water was biogeochemically similar to Phase 1. During Phase 1, temperature was 16.45(0.18)°C, $\Delta(O_2/Ar)$ was 9.8(1.8)%, and macronutrient concentrations were near the analytical detection limits ($[NO_3^-] \leq 0.2$ μmol kg^{-1} for all seven casts and $[SiO_4] \leq 1.0$ μmol kg^{-1} for six out of seven casts) in the upper 4 m. During Phase 2, on average, the surface water had lower temperature (15.88(0.40)°C), lower $\Delta(O_2/Ar)$ (6.7(3.2)%), and higher nutrient concentrations ($[NO_3^-] = 0.5(0.5)$ μmol kg^{-1}, maximum 1.7 μmol kg^{-1} and $[SiO_4] = 1.7(0.8)$ μmol kg^{-1}, maximum 3.0 μmol kg^{-1}), compared to the conditions in Phase 1.

We determined the start time for Phase 2 based on the ship's temperature record; Phase 2 began on 29 September when the sea surface temperature first dropped to 15.91°C, three standard deviations below the mean temperature observed in Phase 1. During the cast on 29 September 06:00, the mixed layer conditions were consistent with the other Phase 1 casts, and beginning with the cast on 29 September 12:00, the mixed layer conditions were more variable. Thus, Phase 2 began sometime between these two casts. The exact start time for Phase 2 does not affect our conclusions. At the beginning of Phase 2 (between the morning of 29 September and 30 September) there was a transition period when cold (~15°C) water with $\Delta(O_2/Ar) \simeq 0\%$ persisted within the study area for several hours. During the rest of the cruise, the water was often colder and had lower O_2 concentrations than in Phase 1, but not as extreme as the conditions during the transition period. This observation suggests that the transition period water was advected out of the study area after the morning of 30 September.

Satellite-based sea surface temperature (SST) measurements supported our shipboard observations of changes in surface water properties in Monterey Bay during the cruise, as well as the presence of strong temperature fronts in Monterey Bay and contiguous waters. On the night of 25 September (prior to the start of the cruise), surface waters within the study area were generally 17–18°C (Figure 2a). There was a patch of

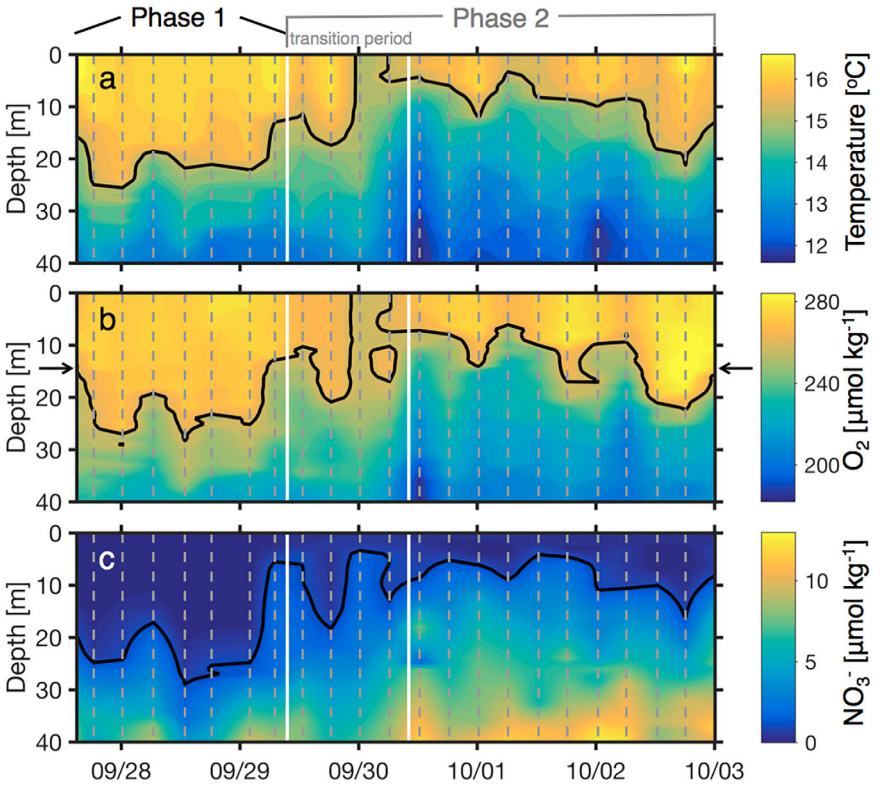

Figure 3. Measured profiles of (a) temperature, (b) [O_2], and (c) [NO_3^-] during the cruise. The black contour lines are at (a) 15.9°C, (b) 260 μmol kg^{-1}, and (c) 1.2 μmol kg^{-1}, and are selected to emphasize the colder water with lower O_2 and higher NO_3^- that entered the euphotic zone during Phase 2. The vertical grey dashed lines show the timing of CTD casts and the vertical white lines are at 29 September 09:35 and 30 September 10:10, the transition period at the start of Phase 2 when the coldest, lowest O_2 surface water passed through the site. The arrows on the *y* axis of (b) indicate the mean O_2-based mixed layer depth (14 m).

colder water (~16°C) at the northwestern edge of the bay, likely a filament of recently upwelled water, but it was outside our main sampling area (Figure 2a). Clouds over Monterey Bay obscured all SST images on the nights of 26–28 September, so we were unfortunately unable to obtain a cloud-free image during Phase 1. By nighttime on 30 September, SST was substantially colder throughout the bay. Our study area overlapped with the coldest water and somewhat warmer water was present to the east and west (Figure 2b).

The above observations are suggestive of lateral advection of recently upwelled water into the study area during Phase 2. The transition between the two phases coincided with the highest total wind speeds and highest southward (upwelling-favorable) wind speeds observed during the cruise [*Manning et al.*, 2016a]. Our data suggest that during Phase 2, we sampled multiple water masses including a colder water mass with lower O_2 and higher nutrients, consistent with recently upwelled water [*Pennington and Chavez*, 2000; *Ryan et al.*, 2009; *Johnson*, 2010], a warmer water mass that had biogeochemical characteristics more similar to Phase 1, and also mixtures of these two water masses. Furthermore, there were often significant difference between the underway and mooring 1 (M1) surface measurements of temperature, [NO_3^-], and [O_2], especially during Phase 2, demonstrating that there was small-scale variability in these parameters within Monterey Bay (Figure 4 for underway data, mooring data not shown). In this paper, we quantify differences in productivity between the two phases, and the impact of these different water masses on productivity estimates in Phase 2.

5.2. ^{14}C Incubations

Here we focus on the incubation results integrated to the mean mixed layer depth for the cruise (14 m, section 4.1). This integration depth is most appropriate for comparison with the O_2-based productivity estimates (section 4.1) [*Hendricks et al.*, 2004; *Hamme et al.*, 2012; *Juranek and Quay*, 2013]. Euphotic zone ^{14}C-PP (to 1% I_o) was on average 11% higher than mixed layer ^{14}C-PP. In supporting information, we include all

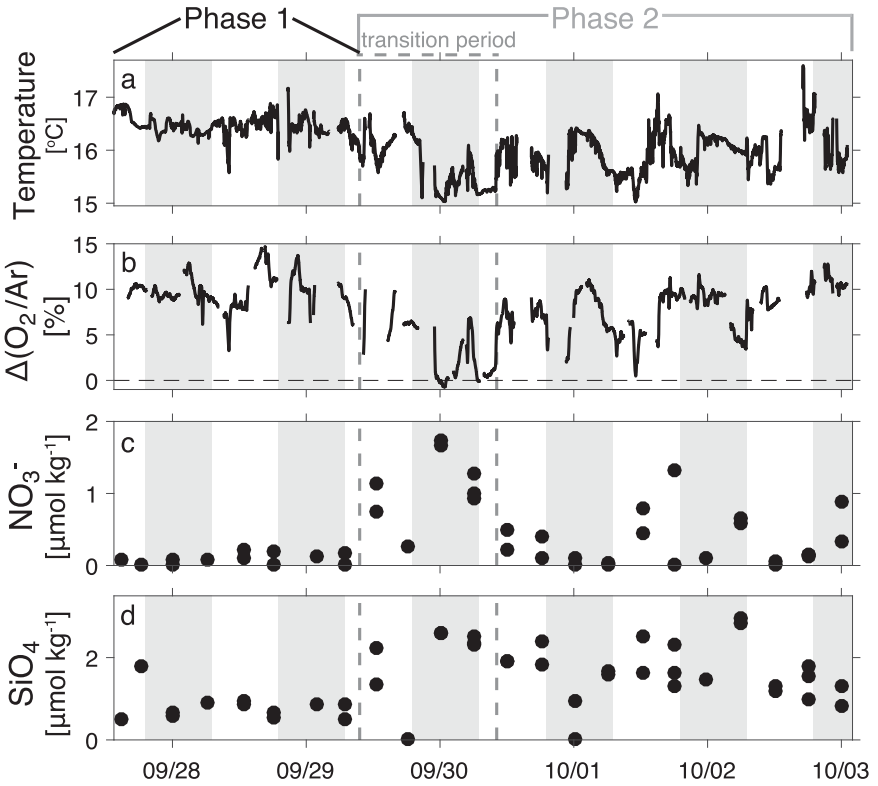

Figure 4. Near-surface (<4 m depth) measurements of (a) temperature from the ship's underway system, (b) $\Delta(O_2/Ar)$ from the underway mass spectrometer, (c) $[NO_3^-]$ from discrete Niskin samples, and (d) $[SiO_4]$ from discrete Niskin samples. The vertical grey dashed lines indicate the transition period at the start of Phase 2 when the coldest, lowest O_2 water passed through the site. The shaded grey bars indicate local nighttime (sunset to sunrise). See supporting information Figures S1 and S2 for the spatial distribution of $\Delta(O_2/Ar)$ and temperature.

incubation results (0.1–100% I_o). We report all results for all methods as mean(± standard deviation) except when noted otherwise.

Because water for the incubations on 29 September was collected at 06:00, when the euphotic zone was warm, had high O_2, and low nutrients, we consider these incubations to be representative of Phase 1. Mixed layer ^{14}C-PP was 96(27) mmol C m^{-2} d^{-1} in Phase 1 and 142(12) mmol C m^{-2} d^{-1} in Phase 2, an increase of 48% (Figure 5c). The first incubation, which was initiated 3 h before sunset on 27 September, is potentially biased somewhat higher (by <30%) than the other incubations which were initiated at dawn [*Pennington et al*., 2015] and therefore is not included in the estimate of Phase 1 ^{14}C-PP. However, we have left the first incubation result in Figure 5c as it shows lower productivity than any of the Phase 2 incubations and strengthens our argument that productivity increased in Phase 2.

5.3. ^{15}N Incubations

During this cruise, the euphotic zone was anomalously warm and low in nutrients compared to prior years, and tracer concentrations were significant relative to ambient conditions (section 3.3). The ^{15}N tracer addition to bottles with low ambient DIN concentrations may have perturbed nutrient cycling within the incubation flasks and potentially caused our incubations to overestimate rates of N uptake and transformations, especially for NH_4^+. This is a common issue for ^{15}N incubations in N-limited marine systems, and with NH_4^+ incubations in general [*Goldman et al*., 1981; *Allen et al*., 1996; *Ward*, 2005].

Despite these potential caveats, our ^{15}N incubation results are generally consistent with the other methods (section 6). In Phase 1, NO_3^- uptake was lower and NH_4^+ uptake was similar, compared to Phase 2 (Figures 5a and 5b). Within the mixed layer, ^{15}N-new production (NO_3^- uptake minus nitrification) was 4.8(1.2) mmol N m^{-2} d^{-1} in Phase 1 and 8.4(1.5) mmol N m^{-2} d^{-1} in Phase 2, an increase of 76% (Table 1). Mixed layer NH_4^+ uptake (^{15}N-regenerated P) was 1.5(0.6) mmol N m^{-2} d^{-1} in Phase 1 and 1.6(0.4) mmol N m^{-2} d^{-1} in Phase 2. Nitrification rates were 2% of NO_3^- uptake rates in Phase 1 and Phase 2. If we assume that NH_4^+

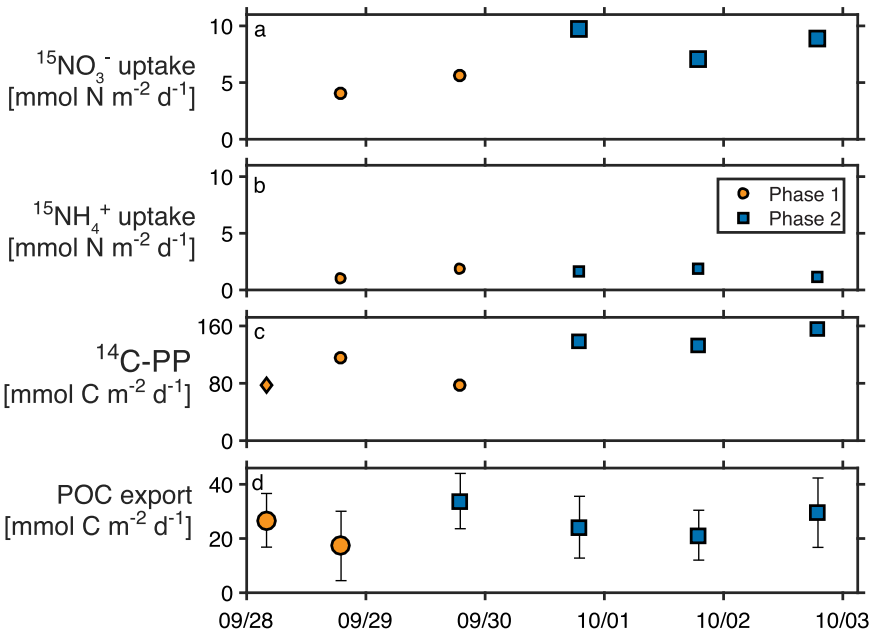

Figure 5. Results of depth-integrated incubations (integrated from 0–14 m depth) measuring (a) $^{15}NO_3^-$ uptake, (b) $^{15}NH_4^+$ uptake, and (c) ^{14}C-PP, as well as (d) sediment trap-based POC flux to 50 m. Orange symbols indicate data representative of Phase 1, and blue symbols show data representative of Phase 2. For Figures 5a–5c, the size of the symbols approximates the measurement error. The first ^{14}C-PP result (orange diamond in Figure 5c) was initiated earlier in the day and therefore may be biased high.

and NO_3^- are the only N sources taken up by phytoplankton, N uptake increased 59% between Phase 1 and Phase 2.

We converted the N uptake to C uptake using a C_{org}:N ratio of 7.3(1.0), the ratio of remineralized organic matter estimated by *Anderson and Sarmiento* [1994]. This ratio is equivalent within uncertainty to the canonical Redfield ratio of 6.6 (averaging phytoplankton and zooplankton) or 7.0 (for phytoplankton) [*Redfield et al.*, 1963], the POC:PN ratio measured in the traps throughout the cruise (7.6(0.3)) and the mean C:N ratio of nutrient-replete phytoplankton cultures reported in a compilation by *Geider and La Roche* [2002] (7.7(2.6)).

The ^{15}N incubation results agree with our observations of higher euphotic zone NO_3^- concentrations in Phase 2 compared to Phase 1, which stimulated NO_3^- uptake relative to NH_4^+ uptake.

Table 1. Mixed Layer Productivity and Nitrification Results (mmol m^{-2} d^{-1})[a]

	Phase 1			Phase 2		
Method	C	N	O_2	C	N	O_2
^{14}C-PP[b]	**96 (27)**	13.1 (3.7)	127 (36)	**142 (12)**	19.4 (1.6)	191 (16)
^{15}N-new P[b,c]	35 (8)	**4.8 (1.2)**	47 (11)	61 (10)	**8.4 (1.5)**	84 (14)
^{15}N-regenerated P[b,d]	11 (4)	**1.5 (0.6)**	14 (6)	11 (3)	**1.6 (0.4)**	15 (4)
^{15}N-nitrification[b,e]	0.8 (0.8)	**0.10 (0.09)**	−0.2 (0.2)	1.4 (1.3)	**0.17 (0.16)**	−0.3 (0.3)
O_2/Ar-NCP	35 (10)	4.9 (1.4)	**47 (14)**	30 (12)	4.2 (1.7)	**41 (16)**
$^{17}\Delta$-GPP[f]	209 (17)	28.6 (2.3)	**343 (37)**	206 (34)	28.2 (4.7)	**344 (57)**
Particle flux[g]	**22 (13)**	3.0 (1.8)	29 (18)	**27 (16)**	3.7 (2.2)	37 (22)

[a]Unless otherwise noted, values are converted between C and N using a C:N molar ratio of 7.3(1.0) [*Anderson and Sarmiento*, 1994] and converted between C and O_2 using a C:O_2 ratio (photosynthetic quotient, PQ) of 1.33 in Phase 1 and 1.35 in Phase 2 based on the ratio of NO_3^-:NH_4^+ uptake (section 4.1). Positive C and N values indicate uptake and positive O_2 values indicate production. Values in bold are the units of the original measurement.

[b]Integrated from 0 to 14 m depth, the mean O_2-based mixed layer depth.

[c] ^{15}N-new P is estimated as $^{15}NO_3^-$ uptake minus nitrification.

[d] ^{15}N-regenerated P is estimated as $^{15}NH_4^+$ uptake.

[e]Nitrification rates are converted from mol N:mol C using a ratio of 1:8.3 [*Dore and Karl*, 1996] and from mol N:mol O_2 using a ratio of 1:−2 based on the reaction chemistry ($NH_4^+ + 2O_2 \rightarrow NO_3^- + H_2O + 2H^+$).

[f]GPP is converted from O_2 to C using GPP = (GOP − 0.19GOP)/PQ with PQ = 1.33 in Phase 1 and PQ = 1.35 in Phase 2.

[g]Measured at 50 m depth.

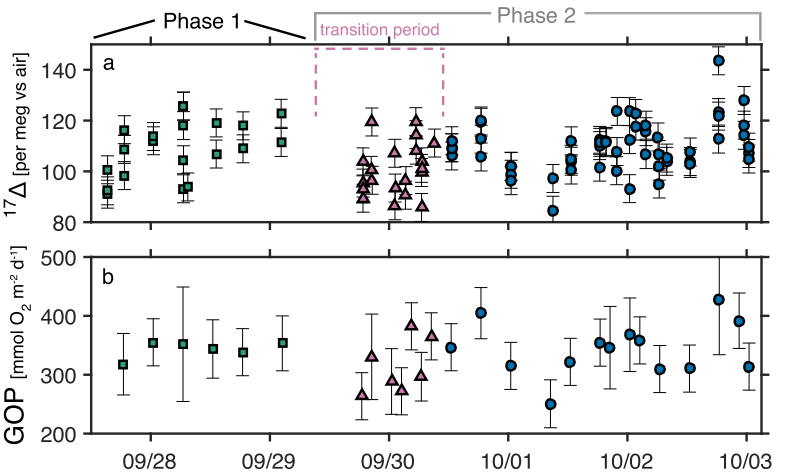

Figure 6. (a) Mixed layer $^{17}\Delta$ ($\lambda = 0.5179$), showing all samples, and (b) steady state GOP, calculated with 2 h bin averaging. The green squares are during Phase 1 and the pink triangles and blue circles are during Phase 2. In Figure 6b, the blue circles were included in the average GOP calculation, and the pink triangles are samples collected during the transition period at the start of Phase 2 when we sampled the coldest, lowest O_2 surface water; we excluded these samples from the Phase 2 average.

5.4. NCP and NOP From O_2/Ar

Throughout Phase 1, $\Delta(O_2/Ar) = 9.8(1.8)\%$ and showed no consistent diurnal cycle, nor any trend with time (Figure 4). Assuming steady state in Phase 1 (i.e., using equation (6)), NOP was 47(14) mmol O_2 m^{-2} d^{-1}. The uncertainty in NOP is calculated by propagating uncertainty in $[O_2]_B$ (18%), k_{w,O_2} (10%, based on the agreement between *Sweeney et al*. [2007] and other recent wind speed-based parameterizations [*Ho et al*., 2006; *Wanninkhof et al*., 2009; *Wanninkhof*, 2014]), and the vertical flux of $[O_2]_B$ (4.6 mmol O_2 m^{-2} d^{-1}, Table 1). Although NOP follows a diurnal cycle [*Johnson*, 2010; *Wilson et al*., 2015], spatial variability in O_2/Ar, lateral transport, and variable rates of vertical mixing may have confounded the observation of a diurnal cycle in O_2/Ar during this time series.

In Phase 2, we measured a larger range of values for surface $\Delta(O_2/Ar)$, with a minimum of -0.7% between midnight and 09:30 on 30 September, and a maximum of 12.8% near sunset on 2 October. The average $\Delta(O_2/Ar)$ in Phase 2 was 6.7(3.2)% beginning at 29 September 09:35 (when the colder water began to enter the study area) or 7.9(2.4)% beginning on 30 September 10:10 (immediately following the transition period, when the coldest water with lowest O_2 concentrations was present in the study area). Steady state NOP beginning on 30 September 10:10 was 41(16) mmol O_2 m^{-2} d^{-1}, which is 14% lower than NOP in Phase 1.

We argue that it is appropriate to exclude the measurements during the transition period between 29 September 09:35 and 30 September 10:10 when calculating NOP because the recently upwelled water sampled at the surface during this period was clearly far removed from steady state. For example, if NOP remained constant throughout the cruise at the rate calculated during Phase 1 and advective O_2 fluxes were negligible, the steady state $\Delta(O_2/Ar)$ in Phase 2 would be 10% (supporting information Figure S3), rather than 0%, the value observed at 30 September 00:00. The steady state $\Delta(O_2/Ar)$ is defined as the saturation state where biological O_2 production and loss to gas exchange and mixing are exactly balanced.

If we assume that NCP increased 48% in Phase 2 (equivalent to the increase in ^{14}C-PP), we would expect $\Delta(O_2/Ar)$ to increase from 0% to 5% between 30 September 00:00 and 3 October 00:00, or to increase from 6% to 9% between 30 September 10:10 and 3 October 00:00 (supporting information Figure S3). The steady state $\Delta(O_2/Ar)$ is 15% and the system would take $\sim$30 days to reach steady state. Even if NOP remained constant in Phase 2, we would expect $\Delta(O_2/Ar)$ to increase by 1–3% by the end of the cruise (supporting information Figure S3). The wide range of measured values of $\Delta(O_2/Ar)$ and the lack of a consistent increase in $\Delta(O_2/Ar)$ during Phase 2 suggests that we were indeed sampling multiple biogeochemically distinct water masses during Phase 2.

Due to the spatial variability in O_2, we were not able to determine the rate of change in $\Delta(O_2/Ar)$ with time, which is needed for a nonsteady state calculation of NOP (equation (5)) [*Hamme et al*., 2012; *Tortell et al*., 2014; *Wilson et al*., 2015; *Palevsky et al*., 2016]. For example, we can calculate a linear regression of $\Delta(O_2/Ar)$

versus time over any 48 h period in Phase 2 (beginning 30 September 10:10 or later), with the 48 h period chosen to prevent diurnal cycling in O_2 from biasing the slope [*Hamme et al.*, 2012]. For the 48 h regressions, the slope ranges from 0.5 to 1.4% d^{-1} (supporting information Figure S4) and the variability in the slope caused by small shifts in the start and end time indicates that we would have low confidence in any nonsteady state term.

Potentially, we could calculate the nonsteady state O_2 flux using only measurements in the recently upwelled water mass, which likely exhibited the biggest change in productivity and $\Delta(O_2/Ar)$. However, we were unable to separate the time series in Phase 2 into different water masses with different histories (supporting information Figure S5). Although the water sampled in Phase 2 ranged from 15.0 to 17.6°C, the salinity range was narrow (most measurements between 33.35 and 33.40 PSS) and a wide range of O_2 saturation anomalies were observed across the range of salinity values (supporting information Figure S5). Temperature in the mixed layer will be strongly affected by surface heat fluxes and cannot be used as a unique water mass tracer [*Price et al.*, 1986; *Cayan*, 1992; *Large et al.*, 1994]. Our high-frequency O_2/Ar data enabled us to detect multiple, biogeochemically distinct water masses within our study area during Phase 2, but our estimated NOP during Phase 2 reported in Table 1, which is based on a steady state calculation (equation (6)), is likely an underestimate as we were unable to calculate the nonsteady state O_2 flux.

If we had continuously sampled within a single recently upwelled filament during Phase 2 (i.e., if we had sampled in a Lagrangian manner), the changes in O_2 would become apparent by the end of the time series and it would be possible to calculate the nonsteady state O_2 flux (supporting information Figure S3). Alternatively, if we had an additional tracer that could be used to separate the time series into different water masses (e.g., NO_3^- or salinity), this would have facilitated our estimation of the nonsteady state O_2 fluxes inside and outside of the filament of recently upwelled water. Finally, if the time series had continued for longer during Phase 2 (i.e., 5–10 days instead of 3 days) and productivity within the recently upwelled filament had continued at a higher rate compared to outside of the filament, the magnitude of the total increase in $\Delta(O_2/Ar)$ (the nonsteady state O_2 flux) within the filament during the observation period would have been larger and may have been easier to quantify, despite the fact that the ship was transiting through different water masses.

5.5. GPP and GOP From $^{17}\Delta$

Using the steady state equation, GOP was 343(37) mmol O_2 m^{-2} d^{-1} in Phase 1 and 334(58) mmol O_2 m^{-2} d^{-1} in Phase 2 beginning at 29 September 09:35, or 344(57) mmol O_2 m^{-2} d^{-1} in Phase 2 beginning at 30 September 10:10 following the transition period, as done for O_2/Ar (Figure 6). The uncertainty in GOP is calculated by propagating the uncertainty in k (10%, section 4.1) and the standard deviation of GOP/$k[O_2]_{eq}$ (equation (8)), after averaging the samples into 2 h bins.

The steady state calculation suggests that GOP was similar in Phase 1 and Phase 2, however, as discussed above for O_2/Ar (section 5.4), O_2 was probably not in steady state during Phase 2, and it is likely that we sampled different water masses with unique biogeochemical characteristics during Phase 2. We did not observe a consistent increase in $^{17}\Delta$ during Phase 2 and therefore were unable to calculate a nonsteady state GOP. We calculated that to generate a 48% increase in GOP in Phase 2 relative to Phase 1 (equivalent to the increase in ^{14}C-PP), we can add a nonsteady state term, $\partial^{17}\Delta/\partial t = 7$ per meg d^{-1} in equation (8). Thus a ~20 per meg increase in GOP between 30 September 10:10 and 3 October 01:00 would be consistent with the observed increase in ^{14}C-PP. Although samples from Phase 2 did not show a steady increase in $^{17}\Delta$ throughout Phase 2, $^{17}\Delta$ was 109(2) per meg on 30 September 12:30, and 118(12) per meg between 2 October 18:30 to 3 October 00:30, an increase of 9 per meg. A small change in $^{17}\Delta$ measured for a short period of time may be indistinguishable from other sources of variability/error, such as the precision of replicate samples (5–7 per meg), the variability within the mixed layer (often greater than 5–7 per meg), diurnal changes in $^{17}\Delta$ [*Sarma et al.*, 2010] and spatial variability in GOP. If the cruise had extended for longer in Phase 2, with GOP maintained at a higher, constant rate, the change in $^{17}\Delta$ would become more apparent with time. When O_2 is at steady state, a 48% difference in GOP is easily distinguishable with the triple oxygen isotope method; for the MLD and wind speed at our study site, a steady state mixed layer GOP = 320 mmol m^{-2} d^{-1} yields $^{17}\Delta \sim 110$ per meg and GOP = 500 mmol m^{-2} d^{-1} yields $^{17}\Delta \sim 150$ per meg. Thus, as for NOP, the steady state estimate of GOP is likely an underestimate of the true GOP in Phase 2.

5.6. Sediment Trap-Based Carbon Fluxes

During the cruise, total particulate organic carbon (POC) content (particles and swimmers) retained on filters gave a gross flux ranging from 31 to 56 mmol C m^{-2} d^{-1} for the six sediment trap deployments. Estimates of the swimmer POC content ranged from 4 to 23 mmol C m^{-2} d^{-1} (8–65% of the total PC flux) for four of the trap deployments. Of the two remaining traps, one gave a swimmer flux exceeding the gross POC flux by 40% but this was removed from the analysis as a negative POC flux is not possible, and on another trap swimmers were not counted. The large spread in the swimmer corrections results in part because we only counted zooplankton in a small fraction of the water (0.1 L out of 4.2 L). Additionally, there is uncertainty in the conversion of the abundances of various zooplankton taxa to their carbon content [*Nozais et al*., 2005].

Considering that swimmer fluxes were not measured on one of the six deployments and there was a large range in swimmer PC estimates, we opted to apply the average swimmer correction of 15(9) mmol C m^{-2} d^{-1} to each daily flux estimate. After this correction, the average PC export flux during the cruise was 25(15) mmol C m^{-2} d^{-1} (range 17–34 mmol C m^{-2} d^{-1}). The flux was 22(13) and 27(16) mmol C m^{-2} d^{-1} in Phase 1 and Phase 2, respectively. In Figure 5, error estimates for each sediment trap are calculated by propagating error from the PC flux measured in the three collection tubes and the uncertainty in the swimmer estimates. For the sediment traps, we consider the incubation beginning on 29 September to be more representative of Phase 2 because it began just a few hours prior to the start of Phase 2. The PC fluxes from all six traps measured at 50 m depth are lower on average than mixed layer (0–14 m) NCP calculated from O_2/Ar and from ^{15}N-new P, but equivalent within methodological uncertainty (Table 1).

6. Synthesis and Comparison With Prior Work

By integrating the results of all the methods, we gain a much more complete understanding of the ecosystem metabolism and carbon cycle state than we would achieve using just one method. We can estimate GPP, NPP, and NCP directly. By difference, we can estimate R_A and R_H, the consumption of organic carbon by autotrophs and heterotrophs, respectively. Furthermore, we can evaluate the agreement between different methods of estimating the same parameters (e.g., NCP from O_2/Ar and NCP from ^{15}N-new P). For comparison purposes, we convert all methods to C units (Table 1) and present the results in an energy flow diagram (Figure 7), which displays the fate of GPP. We only show O_2-based results for Phase 1 in Figure 7 because of the uncertainties in the O_2 mass balance approach during Phase 2.

For example, assuming that ^{14}C-PP and the sum of ^{15}N-new P and ^{15}N-regenerated P uptake both approximate NPP [*Marra*, 2002; *Hendricks et al*., 2005; *Halsey et al*., 2010], we can compare the results of these two methods. Mixed layer NPP from ^{15}N was 47 and 46% lower than NPP from ^{14}C in Phase 1 and Phase 2, respectively. The discrepancy between the ^{15}N and ^{14}C uptake rates suggests that other forms of N such as urea and other DON species were important N sources for phytoplankton [*McCarthy*, 1972; *Bronk et al*., 1994], and/or that a significant portion of the N taken up by phytoplankton was recycled during the 24 h incubations, and/or that the relative contributions of labeled dissolved organic matter on the filters is different for N versus C uptake incubations. Given that N is the limiting nutrient in Monterey Bay [*Kudela and Dugdale*, 2000], we expect dissolved organic matter and nutrient recycling to play a larger role in N uptake relative to C. Temporal decoupling between C

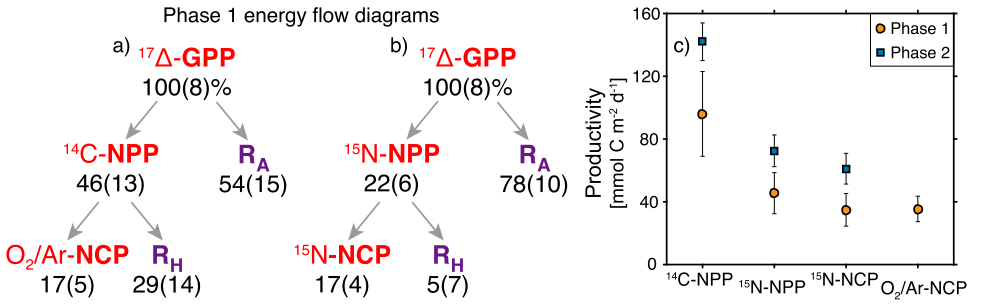

Figure 7. (a and b) Energy flow diagrams for Phase 1, showing the percent of GPP that is respired by autotrophs (R_A), respired by heterotrophs (R_H), remains as NPP, and remains as NCP. (a) GPP, NPP, and NCP are estimated from $^{17}\Delta$, ^{14}C-PP, and O_2/Ar, respectively, and R_A and R_H are estimated by difference. (b) GPP, NPP, and NCP are estimated from $^{17}\Delta$, ^{15}N-NPP and ^{15}N-new P, respectively, and R_A and R_H are estimated by difference. (c) Absolute rates of NPP and NCP. Phase 2 results for O_2/Ar are not shown due to uncertainty in the nonsteady state O_2 flux. All rates are converted to C units as described in Table 1.

fixation and N uptake is another potential cause of discrepancies between simultaneous ^{14}C and ^{15}N incubations. C fixation requires light but some phytoplankton, including diatoms which are a significant primary producer in Monterey Bay, can uptake N in dark and light conditions [*Hutchins and Bruland*, 1995; *Kudela and Dugdale*, 2000; *Clark et al*., 2002]. Although the absolute values of NPP calculated from ^{15}N and ^{14}C are different due to the greater complexity of N cycling, the relative increase in productivity by both methods is nearly identical for Phase 2 relative to Phase 1, suggesting that either method could be used to evaluate temporal trends in NPP.

We can also compare mixed layer NCP calculated from O_2/Ar and the NO_3^- uptake incubations. We assume that NO_3^- uptake minus nitrification yields new production (^{15}N-new P) [*Yool et al*., 2007] and that new production is equivalent to NCP [*Laws*, 1991; *Falkowski et al*., 2003]. In the mixed layer, nitrification decreased new production by 2%. Nitrification rates were higher deeper in the water column and decreased euphotic zone new production (to 1% I_o) by 3–45% (mean 17%, data set DS3). In Phase 1, the methods agreed remarkably well, yielding NCP of 35(8) and 35(10) mmol C m^{-2} d^{-1} from ^{15}N-new P and O_2/Ar, respectively, despite the incubations measuring real-time uptake in bottles and the O_2/Ar technique measuring productivity integrated over approximately 1 week (the residence time of O_2 in the mixed layer). The agreement between the two methods supports our conclusion that O_2 was at steady state in Phase 1. As expected, the particle flux to 50 m measured by the sediment traps (22(13) mmol C m^{-2} d^{-1}) was lower on average than the mixed layer NCP calculated by either method (but equivalent within methodological uncertainty).

In Phase 2, ^{15}N-new P increased to 61(10) mmol C m^{-2} d^{-1} whereas O_2/Ar-based NCP decreased to 30(12) mmol C m^{-2} d^{-1}, according to the steady state calculation. However, we believe that O_2 was not in steady state during Phase 2 and therefore the O_2-based NCP and GPP likely underestimate the true rates (section 5.4).

The frequent measurements of O_2 in Phase 2 enabled insights into the biogeochemical dynamics which were not possible from the daily incubations. All of the 24 h incubations in Phase 2 were initiated at dawn with water from CTD profiles that had measurable near-surface NO_3^- concentrations and low O_2, characteristic of the recently upwelled water. Evaluating O_2 data from all of the CTD casts and underway measurements in Phase 2 showed a wider range of conditions, including both high nutrient, low O_2 surface waters and low nutrient, high O_2 surface waters. Thus the O_2-based approaches, which were used regularly throughout the cruise, provide information on the submesoscale variability in water mass structure and likely productivity within our study site (Figure 4, supporting information Figures S1, and S2). High-frequency productivity data cannot be easily obtained via incubations because they are more labor intensive and because the time of day the incubation is initiated will affect the measured productivity [*Pennington et al*., 2015], confounding the detection of spatial variability.

We can compare our O_2/Ar and $^{17}\Delta$-based estimates of NCP (35(10) mmol C m^{-2} d^{-1}) and GPP (209(17) mmol C m^{-2} d^{-1}) during Phase 1 with other recent studies using these methods in the California Current system. *Munro et al*. [2013] calculated NCP of 27(11) mmol C m^{-2} d^{-1} and GPP of 168(61) mmol C m^{-2} d during October 2006 in inshore California waters near Santa Barbara (termed the "north inshore" region in their study). Our Monterey Bay NCP and GPP are equivalent within uncertainty to these results. *Haskell et al*. [2016b] found mixed layer NCP to be 10(15) mmol C m^{-2} d^{-1} in inshore California waters near Los Angeles during October 2013, lower than NCP during our study. GPP was 230(37) mmol C m^{-2} d^{-1} during the same time period [*Haskell et al*., 2017], which is similar to GPP during our study.

Additionally, *Johnson* [2010] calculated daily NCP using moored near-surface O_2 and NO_3^- sensors at M1 between April and August 2006. He found NCP ranged from approximately −24–48 and −14–53 mmol C m^{-2} d^{-1} when calculated from NO_3^- and O_2, respectively. These results overlap with our Phase 1 estimates of NCP, but our Phase 2 estimate of NCP from NO_3^- uptake incubations is somewhat higher than the corresponding range of results from [NO_3^-] by *Johnson* [2010].

We can also look at ratios of different productivity measures to estimate the ratio of gross to net autotrophic production. Assuming that the 24 h incubations with ^{14}C approximate NPP [*Marra*, 2002], the ratio of GOP/NPP was 3.6(1.1) in Phase 1 and 2.4(0.5) in Phase 2. However, the Phase 2 ratio is likely biased low due to the steady state calculation underestimating GOP. The GOP/NPP ratio in Phase 1 is similar to the GOP/NPP ratio of 3.3 for phytoplankton growing on nitrate measured by *Halsey et al*. [2010], and the ratio of 2.7 observed in incubations from a global compilation of all JGOFS sites [*Juranek and Quay*, 2013]. Since the carbon uptake during this time series was primarily nitrate-driven, we would expect the GOP/NPP ratio to be

Table 2. Productivity Ratios Calculated by Various Methods[a]

Ratio	Calculation Method	Phase 1	Phase 2
GOP/NPP	$^{17}\Delta$-GOP/^{14}C-NPP	3.6(1.1)	2.4(0.5)[b]
NCP/GPP	O_2/Ar-NCP/$^{17}\Delta$-GPP	0.17(0.05)	0.15(0.06)[b]
NCP/GPP	^{15}N-NCP/$^{17}\Delta$-GPP	0.17(0.04)	0.30(0.07)
ef-ratio	^{15}N-NCP/^{15}N-NPP	0.77(0.30)	0.84(0.22)
ef-ratio	^{15}N-NCP/^{14}C-NPP	0.36(0.14)	0.43(0.08)
ef-ratio	O_2/Ar-NCP/^{14}C-NPP	0.37(0.15)	0.21(0.09)[b]

[a] ^{15}N-NCP is estimated as ^{15}N-new P (i.e., ^{15}N-NCP = $^{15}NO_3^-$ uptake − nitrification) as in Table 1. ^{15}N-NPP is estimated from ^{15}N-new P + ^{15}N − regenerated P (i.e., ^{15}N-NPP = $^{15}NO_3^-$ uptake + $^{15}NH_4^+$ uptake − nitrification).
[b] Phase 2 GOP and O_2/Ar NCP are likely too low due to our inability to quantify the nonsteady state O_2 flux.

closer to the nitrate-based (new production) value of *Halsey et al.* [2010] than the JGOFS value, which includes both new and regenerated production. The O_2:C ratio (photosynthetic quotient) of NO_3^- uptake is higher than for NH_4^+ uptake, leading to a higher GOP/NPP ratio for new production [*Laws*, 1991]. In the California Current Ecosystem, *Munro et al.* [2013] calculated a GOP/NPP ratio of ~4.8–8.1 in the north inshore region, using 6 h daytime ^{14}C incubations scaled to 24 h by multiplying by 1.81 [*Eppley*, 1992]. Some of the discrepancy between the GOP/NPP ratio determined in our study and *Munro et al.* [2013] may be due to uncertainty in scaling the incubations from 6 to 24 h.

We also use the ef-ratio = (new production)/NPP = NCP/NPP [*Laws et al.*, 2000] to quantify the fraction of net autotrophic production available for export, and the ratio of NCP/GPP (export efficiency) to quantify the fraction of gross autotrophic production available for export (Table 2). In Phase 1, the ratio of NCP/GPP was 0.17(0.05) and 0.17(0.04) when estimated using $^{17}\Delta$-GPP and NCP from NO_3^- uptake and O_2/Ar, respectively (Figure 7). The ef-ratio was 0.77(0.30) and 0.84(0.22) in Phase 1 and Phase 2, respectively, when calculated assuming that ^{15}N-new P approximates NCP and the sum of ^{15}N-new P and ^{15}N-regenerated P approximates NPP (Table 2). It was 0.36(0.14) and 0.43(0.08) in Phase 1 and Phase 2, respectively, when calculated assuming that ^{15}N-new P approximates NCP and ^{14}C-PP approximates NPP. In Phase 1, the ef-ratio from O_2/Ar-NCP and ^{14}C-PP was 0.37(0.15), equivalent within uncertainty to the result from ^{15}N-new P. In Phase 2, we have less confidence in the O_2-based ef-ratio calculations because the system was not at steady state. Also, the ef-ratio calculated from N uptake only is likely an overestimate throughout the cruise as the NPP estimate does not include additional sources of N such as urea [*McCarthy*, 1972; *Eppley and Peterson*, 1979]. However, our ef-ratio values are similar to other measurements in Monterey Bay based on NO_3^- and NH_4^+ uptake where ef-ratios >0.5 are commonly observed [*Kudela*, 1995; *Olivieri*, 1996; *Kudela and Dugdale*, 2000]. For example, in a modeling study *Olivieri and Chavez* [2000] calculated an annually averaged ef-ratio of 0.84 by this method. These results indicate that as NPP increased during our time series, the ef-ratio also increased.

Finally, the POC flux at 50 m was ~63% of the mixed layer NCP in Phase 1 (from O_2/Ar and ^{15}N, and 44% of the mixed layer NCP in Phase 2 (from ^{15}N-new P), suggesting that roughly half of the mixed layer NCP was respired between ~14 and 50 m. Because we applied the same swimmer correction to all trap measurements, the apparent changes in the ratio of POC export:NCP during our time series must be interpreted with caution. Additionally, the sediment traps underestimate the true OC export since they mainly measure the passively sinking carbon flux and not the other mechanisms of OC export [*Emerson*, 2014].

Given the short duration of our time series, it is not possible to determine the ultimate fate of the organic carbon produced during Phase 2. The incubation results indicate that more organic carbon was available for export from the mixed layer during Phase 2 (i.e., the incubation-based ef-ratio increased). This organic carbon may have been exported vertically locally, advected offshore, or consumed locally. New production and export production are often decoupled in the California Current Ecosystem, and new production typically exceeds export production in coastal waters in this region [*Olivieri and Chavez*, 2000]. For example, the strong horizontal flows in the region can cause organic carbon generated near the shore to be advected laterally rather than sinking vertically at the site of carbon fixation [*Olivieri and Chavez*, 2000; *Plattner et al.*, 2005; *Stukel et al.*, 2011].

7. Implications and Future Directions

Coastal regions impacted by upwelling are a challenging environment in which to quantify oceanic productivity for a variety of reasons. By comparing the results of multiple methods, we demonstrate the conditions under which productivity can be reliably determined by each method. To our knowledge, this is the first

published study that has attempted to compare all of these methods using concurrent measurements in a coastal region.

Monterey Bay, like most of the ocean, is an N-limited system [*Kudela and Dugdale*, 2000; *Moore et al*., 2013]. Some investigators have provided evidence that ^{15}N additions can perturb N cycling and stimulate N uptake in incubations with low-nutrient water, especially for ammonium uptake experiments [*Glibert and Goldman*, 1981; *Allen et al*., 1996; *Ward*, 2005]. Our results demonstrate that NCP calculated from $^{15}NO_3^-$ uptake and from O_2/Ar can give comparable results even in N-limited conditions, when the system is at steady state. The $^{15}NO_3^-$ addition increased total NO_3^- concentration by ~51%, which is significantly higher than typical recommendations to limit tracer addition to ≤10% of ambient concentrations [*Dugdale and Goering*, 1967]. Despite the high N loadings, the two methods of estimating NCP gave results that were equivalent within methodological uncertainty during Phase 1, when NO_3^- concentrations were lower than during Phase 2, but the system was at steady state with respect to O_2 (Table 1).

In Phase 2, our results demonstrate the complementary nature of different approaches. The incubation-based methods can effectively detect short-term changes in a homogeneous system and/or when following a single water mass, but may not measure the mean productivity when sampling a system with significant spatial variability, as we did during Phase 2. In contrast, the high-frequency underway O_2/Ar method integrates over longer timescales and enables the detection of submesoscale variability in water mass structure and potentially productivity. However, the necessity of being in steady state or being able to account for the nonsteady state term can make calculating productivity from O_2/Ar difficult in some systems. Our data reinforce other studies that demonstrate the importance of establishing whether a system is at steady state when using gas tracer-based approaches [*Hamme et al*., 2012; *Tortell et al*., 2014; *Wilson et al*., 2015]. If we only had a single time point measurement of O_2/Ar and $^{17}\Delta$, and did not have productivity estimates from other methods, we would have to assume that the system was at steady state despite having no evidence to support or refute this assumption. Instead, our high-resolution time series measurements of O_2/Ar revealed spatial and temporal variability over the scale of a few km or a few hours during Phase 2 (Figures 4, supporting information Figures S1, and S2). These results provided evidence that the system was not at steady state and that multiple, biogeochemically unique water masses were present within our study area. Additionally, the incubations yield instantaneous, small-scale measurements of productivity and showed that productivity in the recently upwelled waters in Phase 2 was higher than productivity in Phase 1, but incubations were not performed with any water from Phase 2 that had higher O_2 and lower nutrients.

At open ocean time series sites, incubations conducted infrequently (e.g., monthly) can miss sporadic, short-term blooms and periods of high export, whereas investigators have argued that these blooms will be recorded more often by measurements of O_2, which integrates over weeks in the open ocean [*Karl et al*., 2003; *Juranek and Quay*, 2005]. However, in this field study, the phytoplankton bloom during Phase 2 was evident from the incubations, but not the O_2-based methods. During Phase 2, we sampled O_2 both inside and outside a filament of recently upwelled water where O_2 was out of steady state, but all incubations were performed within the recently upwelled filament. The higher nutrient concentrations in this filament initiated a phytoplankton bloom which pushed O_2 further from steady state. The longer integration time of the O_2-based method relative to the length of the time series and the submesoscale variability in surface water properties made it challenging to accurately quantify the increase in NCP and GPP in Phase 2 from these methods. A longer time series would help to resolve these uncertainties. Also, if the different water masses had unique physical and/or biogeochemical properties that were continuously sampled in the underway record (e.g., if the recently upwelled water was significantly higher in salinity and/or if we had continuous underway measurements of $[NO_3^-]$) we could potentially separate the time series into different water parcels and separately quantify productivity in each parcel using our O_2-based methods. In summary, we have demonstrated that ^{15}N-new P incubations and O_2/Ar-based productivity estimates can give comparable results in an N-limited system and that conducting time series measurements of productivity by several methods simultaneously enables a more complete understanding of the ecosystem carbon cycle state than would be achieved by one or two methods alone.

Acknowledgments

Data critical to the conclusions of this study, including incubation results, gas measurements, nutrient measurements, is included in supporting information. MATLAB code for calculating GOP is included in supporting information for this paper and on GitHub (http://github.com/caramanning/calcGOP). MATLAB code for gas diffusivity, solubility, and air-sea fluxes is provided in *Manning and Nicholson* [2016]. Additional data such as CTD profiles, microstructure profiles, and mooring data are available by contacting the lead author (cmanning@whoi.edu). The satellite SST data are available through the NASA Physical Oceanography Distributed Active Archive Center (http://podaac-www.jpl.nasa.gov). We thank Captain Andrew McKee of the R/V Western Flyer and all cruise participants (crew and science team) for a successful cruise. Marguerite Blum (MBARI) analyzed the Winkler O_2 and nutrient samples. Lisa Ziccarelli (MBARI) counted zooplankton swimmers in the sediment traps. Nick Welschmeyer (Moss Landing Marine Labs) provided the sediment traps. Kevin Cahill, Josh Curtice, Bill Jenkins, and Dempsey Lott (WHOI) performed noble gas sample extraction, analysis, and data reduction. Joanne Goudreau (WHOI) assisted with preparation of sample flasks. Zoe Sandwith (WHOI) trained CC Manning on O_2 isotope sample processing and analysis. Chelle Gentemann (Earth and Space Research) provided helpful information on flagging of satellite SST data near fronts. We thank two anonymous reviewers for their constructive comments that improved the manuscript. Mooring data were collected and made available by the Biological Oceanography Group at MBARI. Funding for this work was provided by NSF awards OCE-1060840 to R.H.R. Stanley, OCE-1129644 to D.P. Nicholson, OCE-1357042 to F.P. Chavez, NASA award NNX14AI06G to M.R. Fewings, the David and Lucile Packard Foundation through their generous annual donation to the Monterey Bay Aquarium Research Institute, an Ocean Ventures Fund award from the WHOI Academic Programs Office to CC Manning, and graduate scholarships from NSERC and CMOS to CC Manning.

References

Allen, C. B., J. Kanda, and E. A. Laws (1996), New production and photosynthetic rates within and outside a cyclonic mesoscale eddy in the North Pacific subtropical gyre, *Deep Sea Res., Part I*, *43*(6), 917–936.

Anderson, L. A., and J. L. Sarmiento (1994), Redfield ratios of remineralizationo determined by nutrient data analysis, *Global Biogeochem. Cycles*, *8*(1), 65–80.
Barkan, E., and B. Luz (2003), High-precision measurements of $^{17}O/^{16}O$ and $^{18}O/^{16}O$ of O_2 and O_2/Ar ratio in air, *Rapid Commun. Mass Spectrom.*, *17*(24), 2809–2814.
Barkan, E., and B. Luz (2011), The relationships among the three stable isotopes of oxygen in air, seawater and marine photosynthesis, *Rapid Commun. Mass Spectrom.*, *25*(16), 2367–2369, doi:10.1002/rcm.5125.
Behrenfeld, M. J., and P. G. Falkowski (1997), Photosynthetic rates derived from satellite-based chlorophyll concentration, *Limnol. Oceanogr.*, *42*(1), 1–20.
Behrenfeld, M. J., E. Boss, D. A. Siegel, and D. M. Shea (2005), Carbon-based ocean productivity and phytoplankton physiology from space, *Global Biogeochem. Cycles*, *19*, GB1006, doi:10.1029/2004GB002299.
Bender, M., J. Orchardo, M.-L. Dickson, R. Barber, and S. Lindley (1999), In vitro O_2 fluxes compared with ^{14}C production and other rate terms during the JGOFS Equatorial Pacific experiment, *Deep Sea Res., Part I*, *46*(4), 637–654.
Benson, B. B., and D. Krause (1980), The concentration and isotopic fractionation of gases dissolved in freshwater in equilibrium with the atmosphere. 1. Oxygen, *Limnol. Oceanogr.*, *25*(4), 662–671.
Benson, B. B., and D. Krause (1984), The concentration and isotopic fractionation of oxygen dissolved in freshwater and seawater in equilibrium with the atmosphere, *Limnol. Oceanogr.*, *29*(3), 620–632.
Bond, N. A., M. F. Cronin, H. Freeland, and N. Mantua (2015), Causes and impacts of the 2014 warm anomaly in the NE Pacific, *Geophys. Res. Lett.*, *42*, 3414–3420, doi:10.1002/2015GL063306.
Bronk, D. A., P. M. Glibert, and B. B. Ward (1994), Nitrogen uptake, dissolved organic nitrogen release, and new production, *Science*, *265*(5180), 1843–1846.
Buesseler, K. O. (1991), Do upper-ocean sediment traps provide an accurate record of particle flux?, *Nature*, *353*(6343), 420–423.
Carlson, C. A., H. W. Ducklow, and A. F. Michaels (1994), Annual flux of dissolved organic carbon from the euphotic zone in the northwestern Sargasso Sea, *Nature*, *371*(6496), 405–408.
Carpenter, J. H. (1965), The Chesapeake Bay Institute technique for the Winkler dissolved oxygen method, *Limnol. Oceanogr.*, *10*(1), 141–143.
Carr, M.-E., et al. (2006), A comparison of global estimates of marine primary production from ocean color, *Deep Sea Res., Part II*, *53*(5), 741–770.
Cassar, N., B. A. Barnett, M. L. Bender, J. Kaiser, R. C. Hamme, and B. Tilbrook (2009), Continuous high-frequency dissolved O_2/Ar measurements by equilibrator inlet mass spectrometry, *Anal. Chem.*, *81*(5), 1855–1864.
Cassar, N., P. J. DiFiore, B. A. Barnett, M. L. Bender, A. R. Bowie, B. Tilbrook, K. Petrou, K. J. Westwood, S. W. Wright, and D. Lefevre (2011), The influence of iron and light on net community production in the Subantarctic and Polar Frontal Zones, *Biogeosciences*, *8*(2), 227–237.
Cassar, N., C. D. Nevison, and M. Manizza (2014), Correcting oceanic O_2/Ar-net community production estimates for vertical mixing using N_2O observations, *Geophys. Res. Lett.*, *41*, 8961–8970, doi:10.1002/2014GL062040.
Castro-Morales, K., and J. Kaiser (2012), Using dissolved oxygen concentrations to determine mixed layer depths in the Bellingshausen Sea, *Ocean Sci.*, *8*(1), 1–10.
Cayan, D. R. (1992), Latent and sensible heat flux anomalies over the northern oceans: Driving the sea surface temperature, *J. Phys. Oceanogr.*, *22*(8), 859–881.
Ciais, P., et al. (2013), Carbon and other biogeochemical cycles, in *Climate Change 2013: The Physical Science Basis. Contribution of Working Group I to the Fifth Assessment Report of the Intergovernmental Panel on Climate Change*, edited by J. Fagerberg, D. C. Mowery, and R. R. Nelson, chap. 10, pp. 266–290, Cambridge Univ. Press, Cambridge, U. K.
Clark, D. R., K. J. Flynn, and N. J. Owens (2002), The large capacity for dark nitrate-assimilation in diatoms may overcome nitrate limitation of growth, *New Phytol.*, *155*(1), 101–108.
Craig, H., and T. Hayward (1987), Oxygen supersaturation in the ocean: Biological versus physical contributions, *Science*, *235*, 199–202, doi:10.1126/science.235.4785.199.
Diaz, F., and P. Raimbault (2000), Nitrogen regeneration and dissolved organic nitrogen release during spring in a NW Mediterranean coastal zone (Gulf of Lions): Implications for the estimation of new production, *Mar. Ecol. Prog. Ser.*, *197*, 51–65.
Dore, J. E., and D. M. Karl (1996), Nitrification in the euphotic zone as a source for nitrite, nitrate, and nitrous oxide at station aloha, *Limnol. Oceanogr.*, *41*(8), 1619–1628.
Ducklow, H. W., D. K. Steinberg, and K. O. Buesseler (2001), Upper ocean carbon export and the biological pump, *Oceanography*, *14*(4), 50–58.
Dugdale, R. C., and J. J. Goering (1967), Uptake of new and regenerated forms of nitrogen in primary productivity, *Limnol. Oceanogr.*, *12*(2), 196–206.
Emerson, S. (1987), Seasonal oxygen cycles and biological new production in surface waters of the subarctic Pacific Ocean, *J. Geophys. Res.*, *92*(C6), 6535–6544.
Emerson, S. (2014), Annual net community production and the biological carbon flux in the ocean, *Global Biogeochem. Cycles*, *28*, 14–28, doi:10.1002/2013GB004680.
Emerson, S., P. Quay, and P. A. Wheeler (1993), Biological productivity determined from oxygen mass balance and incubation experiments, *Deep Sea Res., Part I*, *40*(11), 2351–2358.
Emerson, S., P. Quay, D. Karl, C. Winn, L. Tupas, and M. Landry (1997), Experimental determination of the organic carbon flux from open-ocean surface waters, *Nature*, *389*(6654), 951–954.
Eppley, R. W. (1992), Chlorophyll, photosynthesis and new production in the Southern California Bight, *Prog. Oceanogr.*, *30*(1–4), 117–150.
Eppley, R. W., and B. J. Peterson (1979), Particulate organic matter flux and planktonic new production in the deep ocean, *Nature*, *282*, 677–680.
Estapa, M. L., D. A. Siegel, K. O. Buesseler, R. H. R. Stanley, M. W. Lomas, and N. B. Nelson (2015), Decoupling of net community and export production on submesoscales in the Sargasso Sea, *Global Biogeochem. Cycles*, *29*, 1266–1282, doi:10.1002/2014GB004913.
Falkowski, P. G., R. T. Barber, and V. Smetacek (1998), Biogeochemical controls and feedbacks on ocean primary production, *Science*, *281*(5374), 200−206.
Falkowski, P. G., E. A. Laws, R. T. Barber, and J. W. Murray (2003), Phytoplankton and their role in primary, new, and export production, in *Ocean Biogeochemistry*, edited by M. J. R. Fasham, pp. 99–121, Springer, Berlin.
Ferrell, R. T., and D. M. Himmelblau (1967), Diffusion coefficients of nitrogen and oxygen in water, *J. Chem. Eng. Data*, *12*(1), 111–115.
Garcia, H. E., and L. I. Gordon (1992), Oxygen solubility in seawater: Better fitting equations, *Limnol. Oceanogr.*, *37*(6), 1307–1312.
Geider, R., and J. La Roche (2002), Redfield revisited: Variability of C:N:P in marine microalgae and its biochemical basis, *Eur. J. Phycol.*, *37*(1), 1–17.

Giesbrecht, K. E., R. C. Hamme, and S. R. Emerson (2012), Biological productivity along Line P in the subarctic northeast Pacific: In situ versus incubation-based methods, *Global Biogeochem. Cycles*, *26*, GB3028, doi:10.1029/2012GB004349.
Glibert, P., and J. Goldman (1981), Rapid ammonium uptake by marine phytoplankton, *Mar. Biol. Lett.*, *2*, 25–31.
Goldman, J. C., C. D. Taylor, and P. M. Glibert (1981), Nonlinear time-course uptake of carbon and ammonium by marine phytoplankton, *Mar. Ecol. Prog. Ser.*, *6*, 137–148.
Graham, W. M., and J. L. Largier (1997), Upwelling shadows as nearshore retention sites: The example of northern Monterey Bay, *Cont. Shelf Res.*, *17*(5), 509–532.
Grande, K. D., P. J. L. Williams, J. Marra, D. A. Purdie, K. Heinemann, R. W. Eppley, and M. L. Bender (1989), Primary production in the North Pacific gyre: A comparison of rates determined by the ^{14}C, O_2 concentration and ^{18}O methods, *Deep Sea Res., Part A*, *36*(11), 1621–1634.
Grundle, D. S., S. K. Juniper, and K. E. Giesbrecht (2013), Euphotic zone nitrification in the NE subarctic Pacific: Implications for measurements of new production, *Mar. Chem.*, *155*, 113–123.
Halsey, K. H., A. J. Milligan, and M. J. Behrenfeld (2010), Physiological optimization underlies growth rate-independent chlorophyll-specific gross and net primary production, *Photosynth. Res.*, *103*(2), 125–137.
Hamme, R., and S. Emerson (2004), The solubility of neon, nitrogen and argon in distilled water and seawater, *Deep Sea Res., Part I*, *51*(11), 1517–1528.
Hamme, R. C., and S. R. Emerson (2006), Constraining bubble dynamics and mixing with dissolved gases: Implications for productivity measurements by oxygen mass balance, *J. Mar. Res.*, *64*, 73–95, doi:10.1357/002224006776412322.
Hamme, R. C., et al. (2012), Dissolved O_2/Ar and other methods reveal rapid changes in productivity during a Lagrangian experiment in the Southern Ocean, *J. Geophys. Res.*, *117*, C00F12, doi:10.1029/2011JC007046.
Hansell, D. A., and C. A. Carlson (1998), Net community production of dissolved organic carbon, *Global Biogeochem. Cycles*, *12*(3), 443–453.
Haskell, W. Z., M. G. Prokopenko, R. H. R. Stanley, and A. N. Knapp (2016a), Estimates of vertical turbulent mixing used to determine a vertical gradient in net and gross oxygen production in the oligotrophic South Pacific Gyre, *Geophys. Res. Lett.*, *43*, 7590–7599, doi:10.1002/2016GL069523.
Haskell, W. Z., M. G. Prokopenko, D. E. Hammond, R. H. R. Stanley, W. M. Berelson, J. J. Baronas, J. C. Fleming, and L. Aluwihare (2016b), An organic carbon budget for coastal Southern California determined by estimates of vertical nutrient flux, net community production and export, *Deep Sea Res., Part I*, *116*, 49–76.
Haskell, W. Z., II, M. G. Prokopenko, D. E. Hammond, R. H. R. Stanley, and Z. O. Sandwith (2017), Annual cyclicity in export efficiency in the inner Southern California Bight, *Global Biogeochem. Cycles*, *31*, doi:10.1002/2016GB005561, in press.
Hedges, J. I., and J. H. Stern (1984), Carbon and nitrogen determinations of carbonate-containing solids, *Limnol. Oceanogr.*, *29*(3), 657–663.
Hendricks, M. B., M. L. Bender, and B. A. Barnett (2004), Net and gross O_2 production in the Southern Ocean from measurements of biological O_2 saturation and its triple isotope composition, *Deep Sea Res., Part I*, *51*(11), 1541–1561.
Hendricks, M. B., M. L. Bender, B. A. Barnett, P. Strutton, and F. P. Chavez (2005), Triple oxygen isotope composition of dissolved O_2 in the equatorial Pacific: A tracer of mixing, production, and respiration, *J. Geophys. Res.*, *110*, C12021, doi:10.1029/2004JC002735.
Ho, D. T., C. S. Law, M. J. Smith, P. Schlosser, M. Harvey, and P. Hill (2006), Measurements of air-sea gas exchange at high wind speeds in the Southern Ocean: Implications for global parameterizations, *Geophys. Res. Lett.*, *33*, L16611, doi:10.1029/2006GL026817.
Holmes, R. M., A. Aminot, R. Kérouel, B. A. Hooker, and B. J. Peterson (1999), A simple and precise method for measuring ammonium in marine and freshwater ecosystems, *Can. J. Fish. Aquat. Sci.*, *56*(10), 1801–1808.
Hutchins, D., and K. Bruland (1995), Fe, Zn, Mn and N transfer between size classes in a coastal phytoplankton community: Trace metal and major nutrient recycling compared, *J. Mar. Res.*, *53*(2), 297–313.
Jähne, B., G. Heinz, and W. Dietrich (1987), Measurement of the diffusion coefficients of sparingly soluble gases in water, *J. Geophys. Res.*, *92*(C10), 10,767–10,776.
Johnson, K. S. (2010), Simultaneous measurements of nitrate, oxygen, and carbon dioxide on oceanographic moorings: Observing the Redfield ratio in real time, *Limnol. Oceanogr. Methods*, *55*(2), 615.
Jonsson, B. F., S. C. Doney, J. Dunne, and M. Bender (2013), Evaluation of the Southern Ocean O_2/Ar-based NCP estimates in a model framework, *J. Geophys. Res. Biogeosci.*, *118*, 385–399, doi:10.1002/jgrg.20032.
JPL/OBPG/RSMAS (2006a), *GHRSST Level 2P Global Skin Sea Surface Temperature from the Moderate Resolution Imaging Spectroradiometer (MODIS) on the NASA Aqua Satellite, Ver. 1.0*, PO.DAAC, San Diego, Calif., doi:10.5067/GHMDA-2PJ01.
JPL/OBPG/RSMAS (2006b), *GHRSST Level 2P Global Skin Sea Surface Temperature from the Moderate Resolution Imaging Spectroradiometer (MODIS) on the NASA Terra Satellite. Ver. 1.0*, PO.DAAC, San Diego, Calif., doi:10.5067/GHMDT-2PJ01.
Juranek, L. W., and P. D. Quay (2005), In vitro and in situ gross primary and net community production in the North Pacific Subtropical Gyre using labeled and natural abundance isotopes of dissolved O_2, *Global Biogeochem. Cycles*, *19*, GB3009, doi:10.1029/2004GB002384.
Juranek, L. W., and P. D. Quay (2013), Using triple isotopes of dissolved oxygen to evaluate global marine productivity, *Annu. Rev. Mar. Sci.*, *5*, 503–524.
Juranek, L. W., R. C. Hamme, J. Kaiser, R. Wanninkhof, and P. D. Quay (2010), Evidence of O_2 consumption in underway seawater lines: Implications for air-sea O_2 and CO_2 fluxes, *Geophys. Res. Lett.*, *37*, L01601, doi:10.1029/2009GL040423.
Kaiser, J. (2011), Technical note: Consistent calculation of aquatic gross production from oxygen triple isotope measurements, *Biogeosciences*, *8*(7), 1793–1811.
Kana, T. M. (1992), Relationship between photosynthetic oxygen cycling and carbon assimilation in synechococcus WH7803 (cyanophyta), *J. Phycol.*, *28*(3), 304–308.
Kanda, J., E. Laws, T. Saino, and A. Hattori (1987), An evaluation of isotope dilution effect from conventional data sets of ^{15}N uptake experiments, *J. Plankton Res.*, *9*(1), 79–90.
Karl, D. M., J. R. Christian, J. E. Dore, D. V. Hebel, R. M. Letelier, L. M. Tupas, and C. D. Winn (1996), Seasonal and interannual variability in primary production and particle flux at Station ALOHA, *Deep Sea Res., Part II*, *43*(2), 539–568.
Karl, D. M., D. V. Hebel, K. Björkman, and R. M. Letelier (1998), The role of dissolved organic matter release in the productivity of the oligotrophic North Pacific Ocean, *Limnol. Oceanogr.*, *43*, 1270–1286.
Karl, D. M., E. A. Laws, P. Morris, and S. Emerson (2003), Metabolic balance of the open sea, *Nature*, *426*(6962), 32.
Knauer, G. A., J. H. Martin, and K. W. Bruland (1979), Fluxes of particulate carbon, nitrogen, and phosphorus in the upper water column of the northeast Pacific, *Deep Sea Res., Part A*, *26*(1), 97–108.
Kudela, R. M. (1995), Characterization and prediction of planktonic nitrogenous nutrition and new production in Monterey Bay, California: Nutrition and physiological interactions, PhD thesis, Univ. of South. Calif., Los Angeles.
Kudela, R. M., and R. C. Dugdale (2000), Nutrient regulation of phytoplankton productivity in Monterey Bay, California, *Deep Sea Res., Part II*, *47*(5), 1023–1053.

Large, W. G., J. C. McWilliams, and S. C. Doney (1994), Oceanic vertical mixing: A review and a model with a nonlocal boundary layer parameterization, *Rev. Geophys.*, *32*(4), 363–403.
LaRoche, J., and E. Breitbarth (2005), Importance of the diazotrophs as a source of new nitrogen in the ocean, *J. Sea Res.*, *53*(1), 67–91.
Laws, E. A. (1991), Photosynthetic quotients, new production and net community production in the open ocean, *Deep Sea Res., Part A*, *38*(1), 143–167.
Laws, E. A., P. G. Falkowski, W. O. Smith, H. Ducklow, and J. J. McCarthy (2000), Temperature effects on export production in the open ocean, *Global Biogeochem. Cycles*, *14*(4), 1231–1246.
LeGrande, A. N., and G. A. Schmidt (2006), Global gridded data set of the oxygen isotopic composition in seawater, *Geophys. Res. Lett.*, *33*, L12604, doi:10.1029/2006GL026011.
Longhurst, A. R., and W. G. Harrison (1989), The biological pump: Profiles of plankton production and consumption in the upper ocean, *Prog. Oceanogr.*, *22*(1), 47–123.
Loose, B., W. J. Jenkins, R. Moriarty, P. Brown, L. Jullion, A. C. Naveira Garabato, S. Torres Valdes, M. Hoppema, C. Ballentine, and M. P. Meredith (2016), Estimating the recharge properties of the deep ocean using noble gases and helium isotopes, *J. Geophys. Res. Oceans*, *121*, 5959–5979, doi:10.1002/2016JC011809.
Luz, B., and E. Barkan (2000), Assessment of oceanic productivity with the triple-isotope composition of dissolved oxygen, *Science*, *288*, 2028–2031.
Luz, B., and E. Barkan (2005), The isotopic ratios $^{17}O/^{16}O$ and $^{18}O/^{16}O$ in molecular oxygen and their significance in biogeochemistry, *Geochim. Cosmochim. Acta*, *69*(5), 1099–1110.
Luz, B., and E. Barkan (2009), Net and gross oxygen production from O_2/Ar, $^{17}O/^{16}O$ and $^{18}O/^{16}O$ ratios, *Aquat. Microb. Ecol.*, *56*, 133–145.
Luz, B., and E. Barkan (2010), Variations of $^{17}O/^{16}O$ and $^{18}O/^{16}O$ in meteoric waters, *Geochim. Cosmochim. Acta*, *74*(22), 6276–6286.
Luz, B., and E. Barkan (2011), Proper estimation of marine gross O_2 production with $^{17}O/^{16}O$ and $^{18}O/^{16}O$ ratios of dissolved O_2, *Geophys. Res. Lett.*, *38*, L19606, doi:10.1029/2011GL049138.
MacIsaac, J. J., R. C. Dugdale, R. T. Barber, D. Blasco, and T. T. Packard (1985), Primary production cycle in an upwelling center, *Deep Sea Res., Part A*, *32*(5), 503–529.
Manning, C. C., and D. P. Nicholson (2016), gas_toolbox: Updated release for Manning et al. GTWS-7 proceedings, Zenodo, Genève, Switzerland, doi:10.5281/zenodo.46569. [Available at https://github.com/dnicholson/gas_toolbox.]
Manning, C. C., R. H. R. Stanley, D. P. Nicholson, and M. E. Squibb (2016a), Quantifying air-sea gas exchange using noble gases in a coastal upwelling zone, *IOP Conf. Ser. Earth Environ. Sci.*, *88*(6), 3040–3048, doi:10.1088/1755-1315/35/1/012017.
Manning, C. C., R. H. R. Stanley, and D. E. Lott (2016b), Continuous measurements of dissolved Ne, Ar, Kr, and Xe with a field-deployable gas equilibration mass spectrometer, *Anal. Chem.*, *88*(6), 3040–3048, doi:10.1021/acs.analchem.5b03102.
Marra, J. (2002), Approaches to the measurement of plankton production, in *Phytoplankton Productivity: Carbon Assimilation in Marine and Freshwater Ecosystems*, edited by P. J. L. B. Williams, D. N. Thomas, and C. S. Reynolds, pp. 78–108, Blackwell, Cambridge, U. K.
Marra, J. (2009), Net and gross productivity: Weighing in with ^{14}C, *Aquat. Microb. Ecol.*, *56*, 123–131.
McCarthy, J. J. (1972), The uptake of urea by natural populations of marine phytoplankton, *Limnol. Oceanogr.*, *17*(5), 738–748, doi:10.4319/lo.1972.17.5.0738.
Michaels, A. F., M. W. Silver, M. M. Gowing, and G. A. Knauer (1990), Cryptic zooplankton "swimmers" in upper ocean sediment traps, *Deep Sea Res., Part A*, *37*(8), 1285–1296.
Moore, C., et al. (2013), Processes and patterns of oceanic nutrient limitation, *Nat. Geosci.*, *6*(9), 701–710.
Morel, A., and J.-F. Berthon (1989), Surface pigments, algal biomass profiles, and potential production of the euphotic layer: Relationships reinvestigated in view of remote-sensing applications, *Limnol. Oceanogr.*, *34*(8), 1545–1562.
Munro, D. R., P. D. Quay, L. W. Juranek, and R. Goericke (2013), Biological production rates off the Southern California coast estimated from triple O_2 isotopes and O_2:Ar gas ratios, *Limnol. Oceanogr. Methods*, *58*(4), 1312–1328.
Nagai, T., N. Gruber, H. Frenzel, Z. Lachkar, J. McWilliams, and G.-K. Plattner (2015), Dominant role of eddies and filaments in the offshore transport of carbon and nutrients in the California Current System, *J. Geophys. Res. Oceans*, *120*, 5318–5341, doi:10.1002/2015JC010889.
Nicholson, D. P., S. R. Emerson, S. Khatiwala, and R. C. Hamme (2011), An inverse approach to estimate bubble-mediated air-sea gas flux from inert gas measurements, in *Proceedings of the 6th International Symposium on Gas Transfer at Water Surfaces*, Kyoto Univ. Press, Kyoto, Japan.
Nicholson, D. P., R. H. R. Stanley, E. Barkan, D. M. Karl, B. Luz, P. D. Quay, and S. C. Doney (2012), Evaluating triple oxygen isotope estimates of gross primary production at the Hawaii Ocean Time-series and Bermuda Atlantic Time-series Study sites, *J. Geophys. Res.*, *117*, C05012, doi:10.1029/2010JC006856.
Nicholson, D., R. H. Stanley, and S. C. Doney (2014), The triple oxygen isotope tracer of primary productivity in a dynamic ocean model, *Global Biogeochem. Cycles*, *28*, 538–552, doi:10.1002/2013GB004704.
Nieto, K., H. Demarcq, and S. McClatchie (2012), Mesoscale frontal structures in the Canary Upwelling System: New front and filament detection algorithms applied to spatial and temporal patterns, *Remote Sens. Environ.*, *123*, 339–346.
Nozais, C., R. Perissinotto, and G. Tita (2005), Seasonal dynamics of meiofauna in a South African temporarily open/closed estuary (Mdloti Estuary, Indian Ocean), *Estuarine Coastal Shelf Sci.*, *62*(1), 325–338.
Olivieri, R. A. (1996), *Plankton Dynamics and the Fate of Primary Production in the Coastal Upwelling Ecosystem of Monterey Bay, California*, Univ. of Calif., Santa Cruz.
Olivieri, R. A., and F. P. Chavez (2000), A model of plankton dynamics for the coastal upwelling system of Monterey Bay, California, *Deep Sea Res., Part II*, *47*(5), 1077–1106.
Oram, J. J., J. C. McWilliams, and K. D. Stolzenbach (2008), Gradient-based edge detection and feature classification of sea-surface images of the Southern California Bight, *Remote Sens. Environ.*, *112*(5), 2397–2415.
Palevsky, H. I., P. D. Quay, D. E. Lockwood, and D. P. Nicholson (2016), The annual cycle of gross primary production, net community production, and export efficiency across the North Pacific Ocean, *Global Biogeochem. Cycles*, *30*, 361–380, doi:10.1002/2015GB005318.
Pauly, D., and V. Christensen (1995), Primary production required to sustain global fisheries, *Nature*, *374*(6519), 255–257.
Pei, S., and E. A. Laws (2013), Does the ^{14}C method estimate net photosynthesis? Implications from batch and continuous culture studies of marine phytoplankton, *Deep Sea Res., Part I*, *82*, 1–9.
Pennington, J. T., and F. P. Chavez (2000), Seasonal fluctuations of temperature, salinity, nitrate, chlorophyll and primary production at station H3/M1 over 1989–1996 in Monterey Bay, California, *Deep Sea Res., Part II*, *47*(5), 947–973.
Pennington, J. T., K. L. Mahoney, V. S. Kuwahara, D. D. Kolber, R. Calienes, and F. P. Chavez (2006), Primary production in the eastern tropical Pacific: A review, *Prog. Oceanogr.*, *69*(2), 285–317.
Pennington, J. T., M. Blum, and F. P. Chavez (2015), Seawater sampling by an autonomous underwater vehicle: Gulper sample validation for nitrate, chlorophyll, phytoplankton, and primary production, *Limnol. Oceanogr. Methods*, *14*, 14–23.

Peterson, W. T., D. F. Arcos, G. B. McManus, H. Dam, D. Bellantoni, T. Johnson, and P. Tiselius (1988), The nearshore zone during coastal upwelling: Daily variability and coupling between primary and secondary production off central Chile, *Prog. Oceanogr.*, *20*(1), 1–40.

Pilskaln, C. H., J. B. Paduan, F. P. Chavez, R. Y. Anderson, and W. M. Berelson (1996), Carbon export and regeneration in the coastal upwelling system of Monterey Bay, central California, *J. Mar. Res.*, *54*(6), 1149–1178.

Plattner, G.-K., N. Gruber, H. Frenzel, and J. C. McWilliams (2005), Decoupling marine export production from new production, *Geophys. Res. Lett.*, *32*, L11612, doi:10.1029/2005GL022660.

Price, J. F., R. A. Weller, and R. Pinkel (1986), Diurnal cycling: Observations and models of the upper ocean response to diurnal heating, cooling, and wind mixing, *J. Geophys. Res.*, *91*(C7), 8411–8427.

Prokopenko, M. G., O. M. Pauluis, J. Granger, and L. Y. Yeung (2011), Exact evaluation of gross photosynthetic production from the oxygen triple-isotope composition of O_2: Implications for the net-to-gross primary production ratios, *Geophys. Res. Lett.*, *38*, L14603, doi:10.1029/2011GL047652.

Redfield, A. C., B. Ketchum, and F. Richards (1963), The influence of organisms on the composition of sea-water, in *The Sea: Ideas and Observations of Progress in the Study of the Seas. Volume 2, The Composition of Sea-Water*, edited by M. Hill, vol. 2, pp. 26–77, John Wiley, New York.

Reuer, M., B. Barnett, M. Bender, P. Falkowski, and M. Hendricks (2007), New estimates of Southern Ocean biological production rates from O_2/Ar ratios and the triple isotope composition of O_2, *Deep Sea Res., Part I*, *54*, 951–974.

Rosenfeld, L. K., F. B. Schwing, N. Garfield, and D. E. Tracy (1994), Bifurcated flow from an upwelling center: A cold water source for Monterey Bay, *Cont. Shelf Res.*, *14*(9), 931–964.

Ryan, J. P., A. M. Fischer, R. M. Kudela, J. F. Gower, S. A. King, R. Marin, and F. P. Chavez (2009), Influences of upwelling and downwelling winds on red tide bloom dynamics in Monterey Bay, California, *Cont. Shelf Res.*, *29*(5), 785–795.

Sakamoto, C. M., G. E. Friederich, and L. A. Codispoti (1990), MBARI procedures for automated nutrient analyses using a modified Alpkem Series 300 rapid flow analyzer, *Tech. Rep. 90-2*, Monterey Bay Aquarium Res. Inst., Moss Landing, Calif.

Santoro, A. E., C. M. Sakamoto, J. M. Smith, J. N. Plant, A. L. Gehman, A. Z. Worden, K. S. Johnson, C. A. Francis, and K. L. Casciotti (2013), Measurements of nitrite production in and around the primary nitrite maximum in the central California Current, *Biogeosciences*, *10*(11), 7395–7410.

Sarma, V. V. S. S., O. Abe, M. Honda, and T. Saino (2010), Estimating of gas transfer velocity using triple isotopes of dissolved oxygen, *J. Oceanogr.*, *66*(4), 505–512.

Seager, R., M. Hoerling, S. Schubert, H. Wang, B. Lyon, A. Kumar, J. Nakamura, and N. Henderson (2015), Causes of the 2011–14 California drought, *J. Clim.*, *28*(18), 6997–7024.

Siegel, D. A., et al. (2016), Prediction of the export and fate of global ocean net primary production: The EXPORTS Science Plan, *Front. Mar. Sci.*, *3*, 22.

Sigman, D. M., K. L. Casciotti, M. Andreani, C. Barford, M. Galanter, and J. K. Böhlke (2001), A bacterial method for the nitrogen isotopic analysis of nitrate in seawater and freshwater, *Anal. Chem.*, *73*(17), 4145–4153.

Smith, J. M., K. L. Casciotti, F. P. Chavez, and C. A. Francis (2014a), Differential contributions of archaeal ammonia oxidizer ecotypes to nitrification in coastal surface waters, *ISME J.*, *8*(8), 1704–1714.

Smith, J. M., F. P. Chavez, and C. A. Francis (2014b), Ammonium uptake by phytoplankton regulates nitrification in the sunlit ocean, *PLoS One*, *9*(9), e108173.

Smith, J. M., J. Damashek, F. P. Chavez, and C. A. Francis (2016), Factors influencing nitrification rates and the abundance and transcriptional activity of ammonia-oxidizing microorganisms in the dark northeast Pacific Ocean, *Limnol. Oceanogr. Methods*, *61*(2), 596–609, doi:10.1002/lno.10235.

Smith, R. E. H., R. J. Geider, and T. Platt (1984), Microplankton productivity in the oligotrophic ocean, *Nature*, *311*, 252–254.

Spitzer, W. S., and W. J. Jenkins (1989), Rates of vertical mixing, gas exchange and new production: Estimates from seasonal gas cycles in the upper ocean near Bermuda, *J. Mar. Res.*, *47*, 169–196, doi:10.1357/002224089785076370.

Stanley, R. H. R., B. Baschek, D. E. Lott, and W. J. Jenkins (2009), A new automated method for measuring noble gases and their isotopic ratios in water samples, *Geochem. Geophys. Geosyst.*, *10*, Q05008, doi:10.1029/2009GC002429.

Stanley, R. H. R., J. B. Kirkpatrick, N. Cassar, B. A. Barnett, and M. L. Bender (2010), Net community production and gross primary production rates in the western equatorial Pacific, *Global Biogeochem. Cycles*, *24*, GB4001, doi:10.1029/2009GB003651.

Stanley, R. H. R., Z. O. Sandwith, and W. J. Williams (2015), Rates of summertime biological productivity in the Beaufort Gyre: A comparison between the low and record-low ice conditions of August 2011 and 2012, *J. Mar. Syst.*, *147*, 29–44.

Steemann Nielsen, E. (1951), Measurement of the production of organic matter in the sea by means of carbon-14, *Nature*, *167*, 684–685.

Steemann Nielsen, E. (1952), The use of radio-active carbon (C^{14}) for measuring organic production in the sea, *J. Cons. Int. Explor. Mer.*, *18*(2), 117–140.

Steemann Nielsen, E., and E. A. Jensen (1957), Primary oceanic production, *Galathea Rep.*, *1*, 49–135.

Steinberg, D. K., C. A. Carlson, N. R. Bates, S. A. Goldthwait, L. P. Madin, and A. F. Michaels (2000), Zooplankton vertical migration and the active transport of dissolved organic and inorganic carbon in the Sargasso Sea, *Deep Sea Res., Part I*, *47*(1), 137–158.

Stukel, M. R., M. R. Landry, C. R. Benitez-Nelson, and R. Goericke (2011), Trophic cycling and carbon export relationships in the California Current Ecosystem, *Limnol. Oceanogr. Methods*, *56*(5), 1866–1878.

Sweeney, C., E. Gloor, A. R. Jacobson, R. M. Key, G. McKinley, J. L. Sarmiento, and R. Wanninkhof (2007), Constraining global air-sea gas exchange for CO_2 with recent bomb ^{14}C measurements, *Global Biogeochem. Cycles*, *21*, GB2015, doi:10.1029/2006GB002784.

Teeter, L. (2014), Modelling oxygen and argon to improve estimation of net community productivity in a coastal upwelling zone using ΔO_2/Ar, Master's thesis, Univ. of Victoria, Victoria, BC, Canada.

Thiemens, M. H., T. Jackson, E. C. Zipf, P. W. Erdman, and C. van Egmond (1995), Carbon dioxide and oxygen isotope anomalies in the mesosphere and stratosphere, *Science*, *270*(5238), 969–972, doi:10.1126/science.270.5238.969.

Tortell, P. D., E. C. Asher, H. W. Ducklow, J. A. Goldman, J. W. Dacey, J. J. Grzymski, J. N. Young, S. A. Kranz, K. S. Bernard, and F. M. Morel (2014), Metabolic balance of coastal Antarctic waters revealed by autonomous pCO_2 and ΔO_2/Ar measurements, *Geophys. Res. Lett.*, *41*, 6803–6810, doi:10.1002/2014GL061266.

Viviani, D. A., D. M. Karl, and M. J. Church (2015), Variability in photosynthetic production of dissolved and particulate organic carbon in the North Pacific Subtropical Gyre, *Front. Mar. Sci.*, *2*, 73.

Wanninkhof, R. (2014), Relationship between wind speed and gas exchange over the ocean revisited, *Limnol. Oceanogr. Methods*, *12*(6), 351–362.

Wanninkhof, R., W. E. Asher, D. T. Ho, C. Sweeney, and W. R. McGillis (2009), Advances in quantifying air-sea gas exchange and environmental forcing, *Annu. Rev. Mar. Sci.*, *1*, 213–244.

Ward, B. B. (2005), Temporal variability in nitrification rates and related biogeochemical factors in Monterey Bay, California, USA, *Mar. Ecol. Prog. Ser.*, *292*(97), 109.

Weeding, B., and T. W. Trull (2014), Hourly oxygen and total gas tension measurements at the Southern Ocean Time Series site reveal winter ventilation and spring net community production, *J. Geophys. Res. Oceans*, *119*, 348–358, doi:10.1002/2013JC009302.

Wilkerson, F. P., R. C. Dugdale, R. M. Kudela, and F. P. Chavez (2000), Biomass and productivity in Monterey Bay, California: Contribution of the large phytoplankton, *Deep Sea Res., Part II*, *47*(5), 1003–1022.

Williams, P. J. (1993), Chemical and tracer methods of measuring plankton production, *ICES Mar. Sci. Symp.*, *197*, 20–36.

Williams, P. J., and D. A. Purdie (1991), In vitro and in situ derived rates of gross production, net community production and respiration of oxygen in the oligotrophic subtropical gyre of the North Pacific Ocean, *Deep Sea Res., Part A*, *38*(7), 891–910.

Williams, P. J., K. R. Heinemann, J. Marra, and D. A. Purdie (1983), Comparison of ^{14}C and O_2 measurements of phytoplankton production in oligotrophic waters, *Nature*, *305*, 49–50.

Williams, P. J., P. J. Morris, and D. M. Karl (2004), Net community production and metabolic balance at the oligotrophic ocean site, station ALOHA, *Deep Sea Res., Part I*, *51*(11), 1563–1578.

Wilson, S. T., et al. (2015), Short-term variability in euphotic zone biogeochemistry and primary productivity at Station ALOHA: A case study of summer 2012, *Global Biogeochem. Cycles*, *29*, 1145–1164, doi:10.1002/2015GB005141.

Wolk, F., H. Yamazaki, L. Seuront, and R. G. Lueck (2002), A new free-fall profiler for measuring biophysical microstructure, *J. Atmos. Oceanic Technol.*, *19*(5), 780–793.

Woodson, C., L. Washburn, J. A. Barth, D. Hoover, A. R. Kirincich, M. McManus, J. P. Ryan, and J. Tyburczy (2009), Northern Monterey Bay upwelling shadow front: Observations of a coastally and surface-trapped buoyant plume, *J. Geophys. Res. Oceans*, *114*, C12013, doi: 10.1029/2009JC005623.

Wurgaft, E., O. Shamir, and A. Angert (2013), Technical Note: The effect of vertical turbulent mixing on gross O_2 production assessments by the triple isotopic composition of dissolved O_2, *Biogeosciences*, *10*(12), 8363–8371.

Yool, A., A. P. Martin, C. Fernández, and D. R. Clark (2007), The significance of nitrification for oceanic new production, *Nature*, *447*(7147), 999–1002.